Professur für Hydrologie
Fakultät für Umwelt und Natürliche Ressourcen
der Albert-Ludwigs-Universität Freiburg i.Br.

Andreas Lange

Alpine Groundwater

-

Investigations of an Alluvial Aquifer

Masterarbeit unter Leitung von Prof. Dr. Markus Weiler
Freiburg i.Br., März 2015

Professur für Hydrologie
Fakultät für Umwelt und Natürliche Ressourcen
der Albert-Ludwigs-Universität Freiburg i.Br.

Andreas Lange

Alpine Groundwater

–

Investigations of an Alluvial Aquifer

Referent: Prof. Dr. Markus Weiler
Korreferentin: Prof. Dr. Jan Seibert
Wissenschaftliche Betreuung: Dr. Philipp Schneider

Masterarbeit unter Leitung von Prof. Dr. Markus Weiler
Freiburg i.Br., März 2015

Contents

List of Figures

List of Tables

Abbreviations

Symbol	Unit	Description
BF		Base flow
CTD sensor		Sensor for conductivity, temperature & depth (pressure)
DE		Deuterium excess
EC	mS/cm	Electrical conductivity
ERT		Electrical resistivity tomography
GIUZ		Departement of Geography, University of Zürich
GL	m a.s.l.	Ground level
GMWL		Global meteoric water line
GW		Groundwater
HDPE		High density polyethylene
HH	m	Hydraulic head
K_{sat}	m/s	Saturated hydraulic conductivity
LIA		Little Ice Age (End 1850)
LMWL		Local meteoric water line
MAAT	°C	Mean annual air temperature
MDAT	°C	Mean daily air temperature
MWL		Melt water lake (Exfiltration of GW in snowcover)
PTFE		Polytetrafluorethylene
r^2		Correlation coefficient
SLF		WSL Institute of Snow and Avalanche Research SLF
SOF		Saturated overland flow
SWE	mm	Snow water equivalent
T_a	°C	Air temperature
T_{GW}	°C	Groundwater temperature
T_W	°C	Water temperature
TOW		Top of well
VSMOW		Vienna standard mean ocean water
WPW		Water-level proportional water sampler
^2H	δ VSMOV	Deuterium
^{18}O	δ VSMOV	Oxygen-18

Extended Summary

Groundwater recharge, storage dynamics and groundwater quality were investigated for an alpine alluvial aquifer in the catchment of the Tiefenbach in Central Swiss Alps. The aquifer is a sediment-filled overdeeping formed by the Tiefengletscher during the Little Ice Age. Geophysical measurements indicate an aquifer geometry of 140 x 160 m with a depth up to 20 m. Water level, water temperature and electrical conductivity were measured continuously at several monitoring wells. The aquifer shows a constant, nearly linear decrease during the winter month. During the snowmelt, the aquifer becomes completely filled indicating the snowmelt as the dominating recharge source. The groundwater even exfiltrates into the snowpack. Summer month show frequent fluctuations in water level. Rising water level into the unsaturated zone affects high variability in hydrochemistry. Furthermore two different flow systems with different recharges within the aquifer could be detected. Groundwater temperatures show a strong increase up to 10 °C immediately after the aquifer becomes snow free due to the shallow soils and the strong radiation input.

Keywords
alpine groundwater, water storage, alluvial aquifer, groundwater recharge, groundwater quality, groundwater quantity

Zusammenfassung

Im Einzugsgebiet des Tiefenbaches in den Schweizer Zentralalpen wurde ein alluvialer Aquifer hinsichtlich Grundwasserneubildung, Speicherdynamiken und Grundwasserqualität untersucht. Der Grundwasserspeicher ist eine mit Sedimenten gefüllte Geländeübertiefung, die durch den Tiefengletscher während der letzen kleinen Eiszeit entstanden ist. Die Ausdehnung des Aquifers konnte mittels geophysikalischer Untersuchungen auf etwa 140 x 160 m und einer Tiefe von 20 m bestimmt werden. An mehreren Beobachtungsbrunnen wurden der Wasserstand, die Wassertemperatur sowie die elektrische Leitfähigkeit kontinuirlich gemessen. Während der Wintermonate zeigte der Aquifer eine konstante, nahezu lineare Abnahme im Wasserstand. Im Verlauf der Schneeschmelze wurde der Aquifer wieder komplett aufgefüllt. Dies deutet daraufhin, dass die Schneeschmelze den größten Anteil zur Grundwasserneubildung beiträgt. Der Grundwasserspiegel steigt sogar bis in die noch vorhandene Schneedecke an. Während der Sommermonate konnten sehr variable Grundwasserstände festgestellt werden. Ein Anstieg des Wasserspiegels in die ungesättigte Zone scheint Auswirkungen auf die Hydrochemie zu haben. Desweiteren konnten zwei verschiedene Fließsysteme identifiziert werden. Aufgrund der geringmächtigen Böden und dem direkten Strahlungeinfluss stieg die Grundwassertemperatur sofort nach der Schneeschmelze auf bis zu 10 °C an.

1 Introduction

Mountains are often called the world's natural "water towers", as they play an important role in the water cycle. Especially alpine regions, such as the European Alps, contribute overproportionately high runoff (Viviroli et al. 2003, Viviroli & Weingartner 2004). The European Alps also form the headwaters for the major European rivers like Rhine, Rhone, Po & Danube (Tab. 1.1).

Table 1.1: Hydrological relevance of the Alps for the major European rivers like Rhine, Rhone, Po & Danube. (data source: hydrological atlas of Switzerland 2010, Tafel 6.4) (Schneider 2013).

Rivers	**Relative contribution of the Alps to catchment discharge** [%]	**Relative proportion of the Alps to total catchment area** [%]	**Overproportionality of discharge originating from the Alps** [%]
Rhine	34	15	2.3
Rhone	41	23	1.8
Po	53	35	1.5
Danube	26	10	2.6

In alpine catchments there are a lot of different water storages such as glaciers, seasonal snowpacks, lakes or groundwater. Especially the glaciers and the seasonal snowpack lead to a redistribution of winter precipitation to spring and summer runoff (Viviroli et al. 2011). The glaciers even supply the important water during summer droughts, thus when consumption is highest. However, alpine regions are highly sensitive to possible climate changes, such as the present warming trend. Especially snow, glaciers and permafrost are sensitive with respect to changes in atmospheric conditions, because of their proximity to melting conditions (Haeberli & Beniston 1998). The strong warming rate, especially in summer is crucial for the present glacier retreat (Rebetez & Reinhard 2007). With ongoing glacier retreat and an earlier snowmelt, the significance of glaciers & seasonal snowpacks as storages will be further reduced (Barnett et al. 2005). Retreating glaciers leave their marks in the landscape, such as moraines, talus & bed depressions. These bed depressions are typically found in formerly glaciated areas as a result of the erosive power of glaciers. If such bed depressions are persistent and are filled with melt waters, new lake occurs in the periglacial landscape (Linsbauer et al. 2012). However, in case of enhanced erosion rates, these depressions will most probably be filled with sediments, thus a new unconsolidated aquifer may emerge. These aquifers may partially compensate the reduction of the ice and snow storage, as they act as a new reservoir. Hence, alpine groundwater could play a decisive role in the future. We define alpine groundwater as subsurface storage above the timberline (in the Swiss Alps approximately 2000 m a.s.l.). Despite the importance of alpine groundwater, the system understanding of such aquifers is limited due to a lack of investigations.

Most studies are focused on a single aspect of the hydrological cycle, such as glacier mass balance or snow accumulation and melt (Hood & Hayashi 2015). Moreover, only 3 % of the hydrogeological publications have a direct link to the alpine region and only a few of them are focusing on alpine hydrogeology as the main aspect (Goldscheider 2011). Similarly, the distribution of runoff-, precipitation- & groundwater gauges in Switzerland is highly dependent on the altitude with a strong focus on the mid- and lowlands (Fig. 1.1).

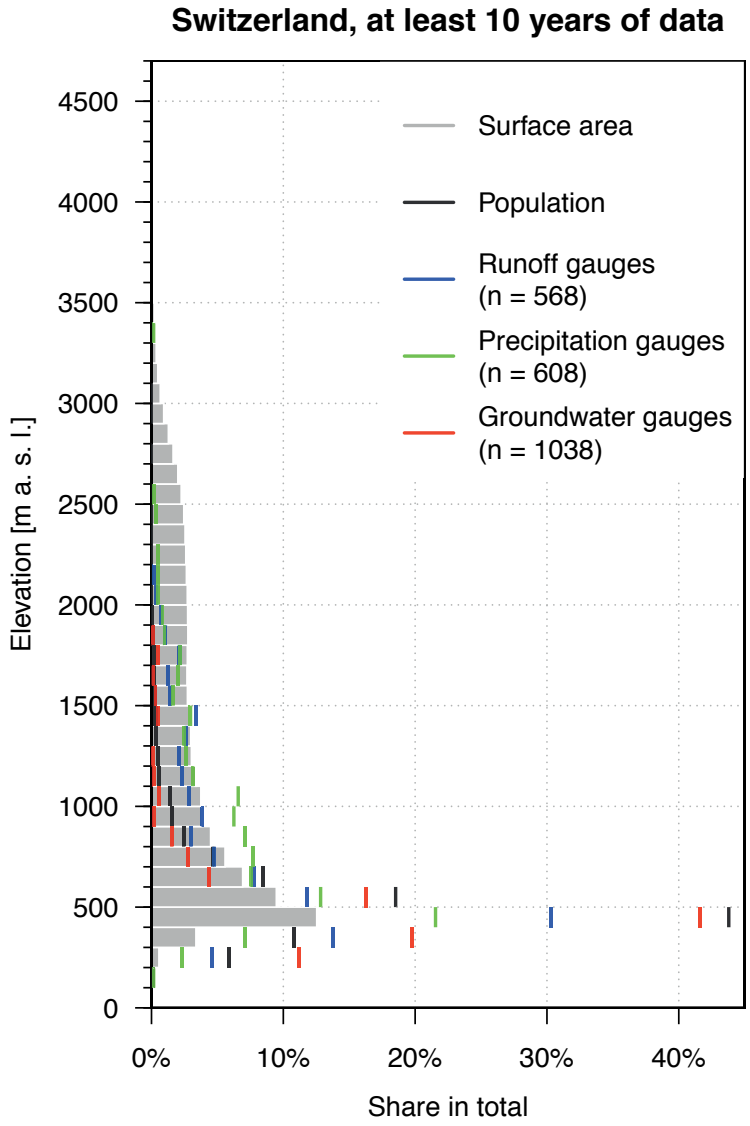

Figure 1.1: Altitudinal distribution of runoff-, precipitation- & groundwater gauges in Switzerland compared to hypsography (modified after Viviroli et al. (2011)). The distribution of groundwater gauges shows a clear correlation with part of population for each altitude zone. This leads to a scarcity of groundwater data in elevations $>$ 1500 m a.s.l., whereby 37 % of the surface area in Switzerland are above this height (Viviroli et al. 2011).

Aquifers above 2000 m a.s.l. are rarely monitored in Europe. Reason for this lack are for example the complicated access and the complex and heterogene geology. Thus, the alpine settings limit the applicability of established hydrogeological methods and approaches and thus makes field instrumentation, field experiments & modeling challenging (Goldscheider 2011).

In addition, a long and cold winter season challenges instrumentation and limits time for field experiments. In alpine regions, recent unconsolidated sediments are typically coarse and poorly sorted (e.g. talus, moraines & alluvial deposits). The coarser sediments and the steep slopes also led to the assumption that the water storage capacity in alpine regions is negligible (Clow et al. 2003). Groundwater recharge and seasonal storage of aquifers in alpine terrain is typically neglected in hydrological models (Schneider 2013). As already mentioned above, the retreat of the glaciers can induce new groundwater reservoirs. These storages can be moraines, talus or alluvial aquifers. Clow et al. (2003) found that for an alpine watershed in the Rocky Mountains, talus fields can contribute more than 75 % to streamflow during the fall and winter base flow period. Talus slopes are the primary groundwater storage at that site, having a maximum storage capacity approximately equal to that of total annual discharge from the catchment. Hood & Hayashi (2015) found similar groundwater storage capacities for an alpine watershed in British Columbia, Canada. McClymont et al. (2010) studied an alpine meadow-talus complex, getting annual recharge from snowmelt and rainfall which is several times higher than the storage capacity. Roy & Hayashi (2008) found, that talus fields and moraines which are in contact with lake shores affect substantial the groundwater exchange with the lakes. The hydrological importance of an alpine alluvial aquifer for flood-buffering and storage is highlighted in Lauber et al. (2014). Ofterdinger et al. (2004) investigated deep groundwater in fractured granite, sampling groundwater in the Bedretto Tunnel, which goes through the granite body of the western Gotthard Massif. They found, that accumulated winter precipitation and glacial meltwater may contribute significantly to recharge of deep groundwater. Due to the scarcity of field studies and their data from alpine groundwater reservoirs, it is challenging to integrate these reservoirs into hydrological models (Tague & Grant 2009). Roy & Hayashi (2009) found multiple distinctive groundwater flow systems within a single moraine-talus field. Thus, it is maybe necessary to use more complex structures within hydrological models. Magnusson et al. (2012) investigated stream-groundwater interactions on the adjacent glacier forefield of Dammagletscher. They determined daily fluctuations in groundwater levels as well as slowly declines over the season. A diffusion model was used to describe the groundwater fluctuations, but the result highlights, that further work is needed to improve the calibration for such heterogeneous field sites like glacier forefields.

All these studies highlight, that alpine groundwater reservoirs may affect significantly the waterbalance of alpine watersheds. It becomes also evident, that the groundwater storages are highly heterogeneous. Therefore, the implication of alpine groundwater reservoirs in hydrological models is considerably more challenging than for most of the lowlands. To our knowledge, none of these studies measured continuously groundwater level fluctuations as well as the electrical conductivity for an alpine groundwater reservoir throughout the winter season. Thus, to improve the understanding of processes and impacts of climate change on alpine water resources, more detailed studies are needed.

2 Problem definition & objectives

This study was conducted as part of the present research project called "Alpine Groundwater - pristine aquifers under threat?" [Forschungskredit Uni Zürich, Research Plan | Dr. Philipp Schneider (Hydrology & Climate, Departement of Geography)]. The initial data series, which could be seen as the impetus for the project is presented in the following figure.

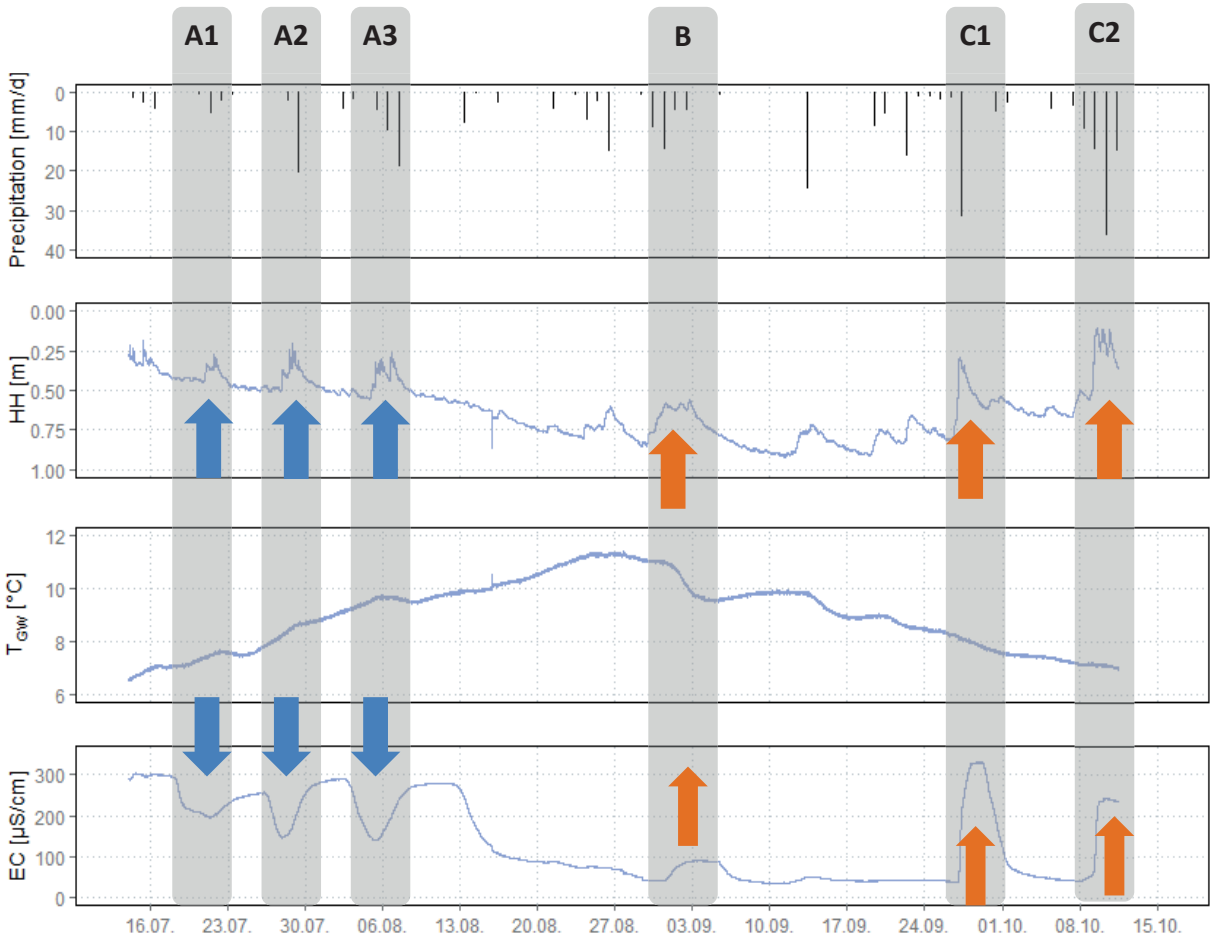

Figure 2.1: Results of pilot study (07/2012 - 10/2012): mean daily precipitation (P), hydraulic head (HH, depth to groundwater), groundwater temperature (T_{GW}) and electrical conductivity (EC); HH, T_{GW} and EC measured in 5 min time steps at test site Tiefenbach floodplain (2365 m, near Albert-Heim SAC hut, Canton Uri). Simultaneously with precipitation events A1, A2 & A3 HH and T_{GW} increased, whereas EC decreased, indicating groundwater recharge from precipitation. During event B precipitation changed from rain to snow and T_{GW} dropped significantly and EC unexpectedly increased. Coincident with precipitation events C1 and C2 T_{GW} continued to decrease while EC increased significantly (Schneider 2013).

Fig. 2.1 shows precipitation events (A1, A2, A3) that accompany with decreasing electrical conductivity (EC). This could be expected cause of the dilution effect. Some precipitation events (B, C1, C2) though indicate rapid and strong increase in EC. Groundwater temperatures (T_{GW}) of more than 11 °C in a height of 2365 m a.s.l. are also striking. It is usually assumed, that groundwater temperature reflects more or less the mean annual air temperature (MAAT) of an area.

Because of the sparse instrumentation of these remote areas, this project can be seen as a first pilot study of alpine porous aquifer observations. The aim of the project is to get a better understanding and conceptualization of processes and reservoirs in alpine terrain to predict the impact of a melting cryosphere on alpine water quality and quantity (Schneider 2013).

The main questions of this thesis are:

1. How do snowmelt, glacial stream and summer precipitation contribute to groundwater recharge?
2. Does the water level fluctuations affect the high variations in electrical conductivity?
3. What is the reason for such high groundwater temperatures?
4. Is it possible, that alpine porous aquifers may compensate the reduction of the glacier contribution to low flows in alpine watersheds?

3 Site description

The study catchment is located near the Furka pass road in the upper Urseren Valley (Canton Uri) in the Central Swiss Alps (Fig. 3.1).

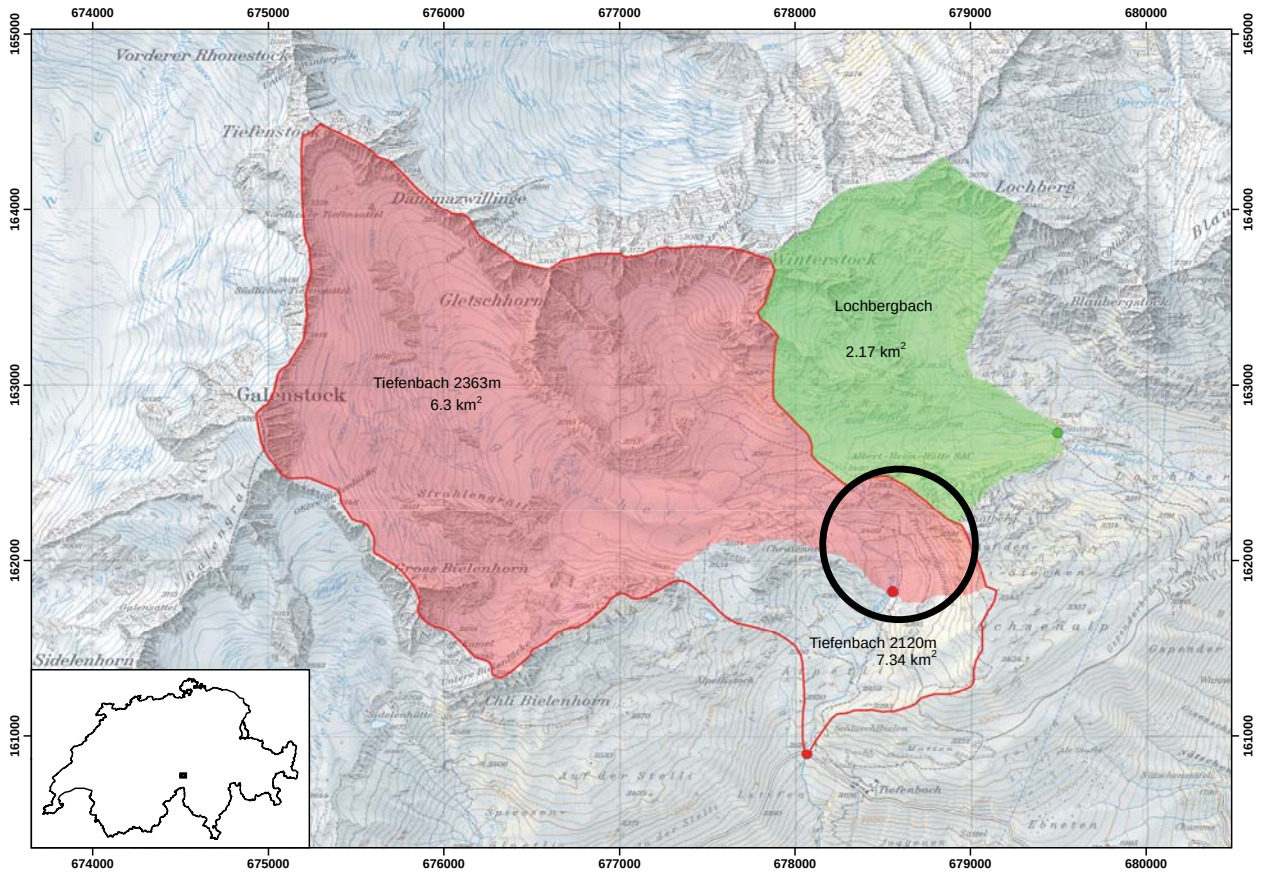

Figure 3.1: Location of test site in the Urseren Valley (Canton Uri, Switzerland) (left corner) and the catchment area (6.3 km^2) of the test site (red colored). The black circle shows the test site and the corresponding catchment outlet (2362.44 m a.s.l.) is symbolized with a red point. The catchment area is bordering the catchment of Lochbergbach in east, Dammagletscher in north and Rhonegletscher in west (Schneider & Lange (2014)).

The catchment area is about 6.3 km^2, with altitudes ranging from 2365 to 3586 m a.s.l. (Galenstock). The catchment area borders the catchment of Lochbergbach in east, Dammagletscher in north and Rhonegletscher in west. The present-day ice cover is about 40 %, whereby the Tiefengletscher has retreated continuously since the Little Ice Age (LIA) in 1850 (Moll 2012). Its meltwater is collected by the Tiefenbach, which drains into the Furkareuss, a tributary of the Reuss river. At the catchment we focused on a sediment-filled depression formed during the LIA at 2365 m a.s.l., about 1 km downstream of the glacier snout (black circle in Fig. 3.1). This sediment-filled depression constitute an alluvial aquifer, where still active deposition through the glacial stream is ongoing. The results from a first geophysical survey in 2012 with electrical resistivity tomography (ERT) show, that this alluvial aquifer is about 20 m deep, 140 wide and 160 long. The alpine terrain is dominated by glacial moraine and alluvial deposits, talus and exposed bedrock (see Fig. 3.2).

Figure 3.2: Photo of the test site. The photo is taken from end moraine of the LIA facing to north-west. The floodplain with our instrumentation is visible on the right site. In the background there is the Tiefengletscher and the Galenstock (3586 m a.s.l.), which is the highest point in the catchment. The glacial stream flows through the center of the image. (photo: Schneider, 2013)

This photo shows the terrain of test site. In the foreground you can see part of the end moraine from the LIA. On the right side you can see the floodplain with some of the instrumentation. The glacial stream flows through the center of the image, originating at the Tiefengletscher, which can be seen at the background.

3.1 Geological & pedological settings

The study catchment is situated on the crystalline Aar massif. The dominating rock type is the Central Aar Granite (Hosein et al. 2004). Fig. 3.3 represents the geology of the test site. The floodplain is characterized through alluvial depositions (still present). Due to the height about 2000 m and the sparse vegetation, the soils are very thin. According to the *World Reference Base for Soil Resources* (WRB 2006) the soils at Tiefenbach floodplain could be classified as *Hyperskeletic Leptosols*. Fig. 3.4 highlights areas with slopes $< 5\,^{\circ}$ respectively $5\,^{\circ}$ - $10\,^{\circ}$. It can be noticed, that areas with slopes $< 5\,\%$ can be often detected in formerly glaciated areas. These aquifers are mostly sediment filled bed depressions. These depressions are a result of the erosive power of glaciers (Linsbauer et al. 2012).

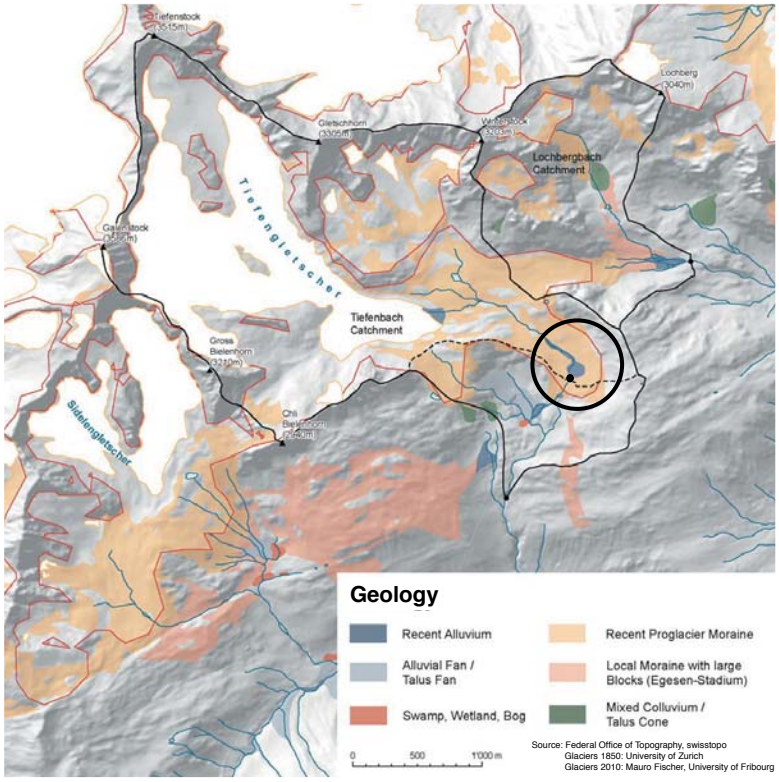

Figure 3.3: Geological map of the Furka test site. Our test site (black circle) is situated at the final glacial extent from the LIA 1850 (red bordered). The geology at the test site is shown as recent proglacial moraine and recent alluvium from the glacial stream (Schneider & Lange (2014)).

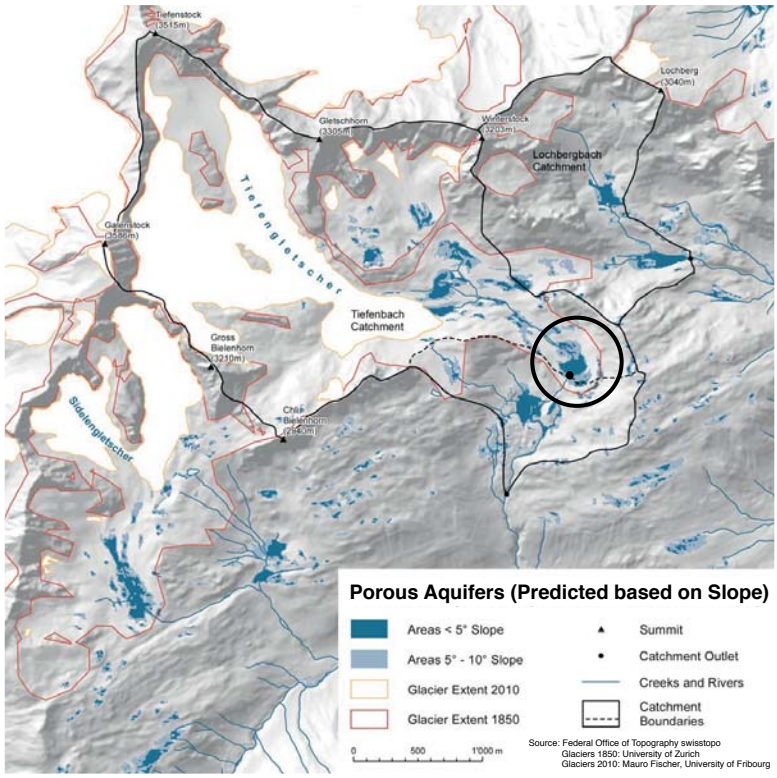

Figure 3.4: Areas with slopes $< 5^\circ$ or 5° - 10°, respectively. In these areas a potential porous aquifers could be formed. The glacial extent from the LIA 1850 (red bordered) indicates, that these potential porous aquifers can be found mainly in formerly glaciated areas (Schneider & Lange (2014)).

3.2 Climatological settings

According to the *Hydrological Atlas of Switzerland* (2010), the mean annual precipitation amount for the period 1951 - 1980 is about 2800 - 3200 mm, whereas the mean annual evaporation is about 200 - 300 mm. The flow-regime can be regarded as a-glacio-nival. The floodplain is typically covered with snow for around 7 - 8 months of the year.

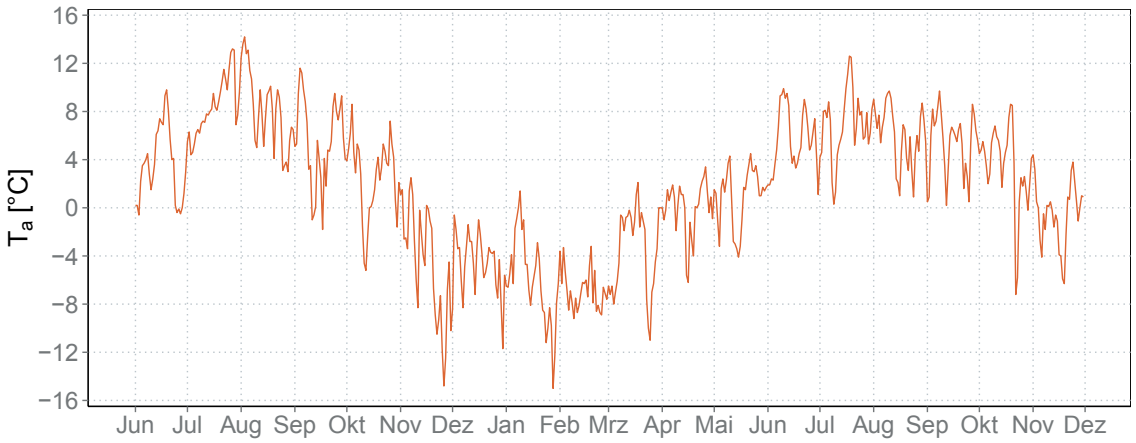

Figure 3.5: Mean daily air temperature (T_a) for Tiefenbach floodplain 06/2013 - 11/2014.

Fig. 3.5 shows the course of mean daily air temperature (T_a) at the test site for 06/2013 untill 11/2014. The mean annual air temperature (MAAT) for the hydrological year (01.10. - 30.09.) 2014 is about 0.2 °C. The nearby station Gütsch ob Andermatt (2283 m a.s.l.) shows for the normperiod 1961 - 1990 a MAAT of −0.5 °C and for the normperiod 1981 - 2010 0.4 °C (MeteoSwiss 2015) (Tab. 3.5).

Table 3.1: Climatological settings of the test site; mean annual air temperature (MAAT) for the hydrological year 2014 (recorded at the test site, 2365 m a.s.l.) as well as the MAAT, snow/rain ratio & mean times of snowcover for the nearby station Gütsch ob Andermatt (2283 m a.s.l.) for climate normal 1961 - 1990 as well as 1981 - 2010 (data source: MeteoSwiss, climate normals); precipitation [mm], evapotranspiration [mm] & flow-regime (*Hydrological Atlas of Switzerland* 2010).

MAAT test site (2014) [°C]	0.2
MAAT Gütsch ob Andermatt (climate normal: 1961 - 1990) [°C]	-0.5
MAAT Gütsch ob Andermatt (climate normal: 1981 - 2010) [°C]	0.4
Precipitation (1951 - 1980) [mm/a]	2800 - 3200
Ratio snow / rain	∼ 2:1
Evapotranspiration (1973 - 1992) [mm/a]	200 - 300
Discharge [mm/a]	2500 - 3300
Mean time of snow cover [month]	7 - 8
Flow regime	a-glacio-nival

4 Methods

4.1 Tracer methods

Different major ions, silica as well as the stable isotopes of water oxygen-18 (^{18}O) and deuterium (^{2}H) were used as tracers. These methods will be presented in the following section.

Major ions

Major ions are, as well as silica, often used as a geochemical tracer. They are primarily used to determine the fraction of water flowing along different subsurface flow paths (Kalbus et al. 2006). In this study, major ions were used to identify the reason for the high fluctuations in EC.

Silica

Dissolved silicic acid is a often used geogenic tracer in hydrology. Based on this it is possible to estimate the origin and resistance time of water. During silicate weathering silicic acid gets constantly free and will be solved in the water. The longer water is in contact with the rock, the higher the concentration of dissolved silicic acid. With the analysis of silica it is also possible to define melt- or event water from the base flow, because silica occurs in precipitation only in very small concentrations (Wels et al. 1991, Kienzler 2001).

Stable isotopes

In hydrology the stable isotopes of water, deuterium (^{2}H) and oxygen-18 (^{18}O), play a decisive role. Since they are a natural part of the water molecule, they can be regarded as an ideal hydrological tracer (Moser et al. 1980, Leibundgut & Seibert 2011). The different atomic mass and physical properties of the different isotopes causes an isotopic fractionation during physical processes, such as evaporation, condensation and freezing. That means, that the isotopic ratio changes over time of the process. By measuring the isotope ratios ^{18}O / ^{16}O and ^{2}H / ^{1}H it is possible to draw conclusions on the origin and age or residence time of the water. Another important parameter in addition to the ^{18}O and ^{2}H values is the deuterium excess (DE). It represents the ratio of the two stable isotopes to each other. Comparing global isotope samples with each other, it is evident that ^{18}O and ^{2}H are in a certain ratio to each other. If you plot ^{18}O against ^{2}H, then all the values plot approximately on a straight line, called *Global Meteoric Water Line* (GMWL). According to Craig (1961), the relation between ^{18}O and ^{2}H can be described as follows:

$$\delta D = 8 \cdot \delta^{18}O + 10 \tag{1}$$

Due to local climatic conditions, e.g. high evaporation rates, and the different origins of the precipitation, a deviation from the GMWL can occur. This deviated line is called *Local Meteoric Water Line* (LMWL). Furthermore, it is possible to detect different effects based on the global distribution of the isotope ratios (Kendall & McDonnell 1998). The preferred condensation of heavier isotopes leads to a progressing depletion of the heavy isotopes during a precipitation event. The precipitation thus will become isotopic lighter with increasing duration of the precipitation event (amount effect). The higher the temperature, the isotopic heavier the precipitation. This is not only important during condensation - i.e. the precipitation event itself - but also during the evaporation. Humid air masses that come from lower latitudes are in fact of that isotopic heavier than those formed at higher latitudes. In addition to the temperature, the humidity at the point of origin plays a decisive role as well (Jouzel & Merlivat 1984) (temperature/latitude effect). Additionally, increasing altitude lead to a depletion of the heavy isotopes, because they condense first (altitude effect). This could be explained by the cooling of the rising air masses and with increasing precipitation amount upwards. Therefrom it represents a combination of amount and temperature effect. Schürch et al. (2003) found an average decrease of ^{18}O in precipitation for the Swiss Alps of about 0.2 ‰ / 100 m. According to the amount and altitude effect it is possible to describe the continental effect. The humid air masses formed over the oceans are first depleted of heavy isotopes in the course of their journey across the continental landmass. Thus, the precipitation with increasing distance to the source is isotopic lighter (Kendall & McDonnell 1998, Moser et al. 1980). Since the isotopic composition of the water differs around the world, a reference standard, called VSMOW (*Vienna Standard Mean Ocean Water*) was introduced. The VSMOW is based on a mixture of several ocean samples and thus represents a uniform reference against which waters of different composition can be compared.

4.2 Field methods

4.2.1 Instrumentation

Water level, water temperature and electrical conductivity (EC) were measured at seven groundwater monitoring wells (15 min interval) and three discharge stations (5 min interval) using online CTD-sensors (**c**onductivity, **t**emperature, **d**epth) from *HT-Hydrotechnik GmbH* (HT). These sensors measured electrical conductivity (accuracy $< 1\,\%$), water temperature (accuracy $< 1\,°C$) and pressure (accuracy $< 0.05\,\%$). The wells consisted partly of HDPE, some of stainless steel and one older one of steel, extending to depths between 0 to 1 m and 2 to 3 m (Fig. 4.1). The sites for the monitoring wells GW1, GW2 & GW3 were selected in such a way that they build an hydrological triangle (see Fig. 4.2). GW2 is located in a depression (2365.05 m a.s.l.), which can easily be distinguished based on the vegetation, because it is saturated almost the whole summer period. In contrast, GW1 is located on a small rise (2365.7 m a.s.l.).

Due to higher variability in EC at monitoring well GW1, two additional wells were installed at this site. GW6 is a deeper one and GW8 is filtered on the first meter (see Fig. 4.1). Next to monitoring well GW1, GW2 & GW3 two mini-piezometers each were installed. A shallow one (P_S) is filtered in 30 - 40 cm depth and a deep one (P_D) at a depth of 90 - 100 cm depth. There are no sensors installed, due to the small inner diameter. The mini-piezometers were only used to get the possibility of sampling in different soil/sediment layers. At previous installations a hard layer at depths of about 0.4 m and 0.7 m was detected. Additionally, two more wells closer to the glacial stream (GW7 & GW9) were installed to quantify the impact of the glacial stream to the aquifer. There were no sensors on GW4 and GW5, since they were no longer used. Continuous measurements in glacial stream upstream of the floodplain were unfortunately not possible. Previous installation attempts were destroyed during higher runoffs (Moll 2012).

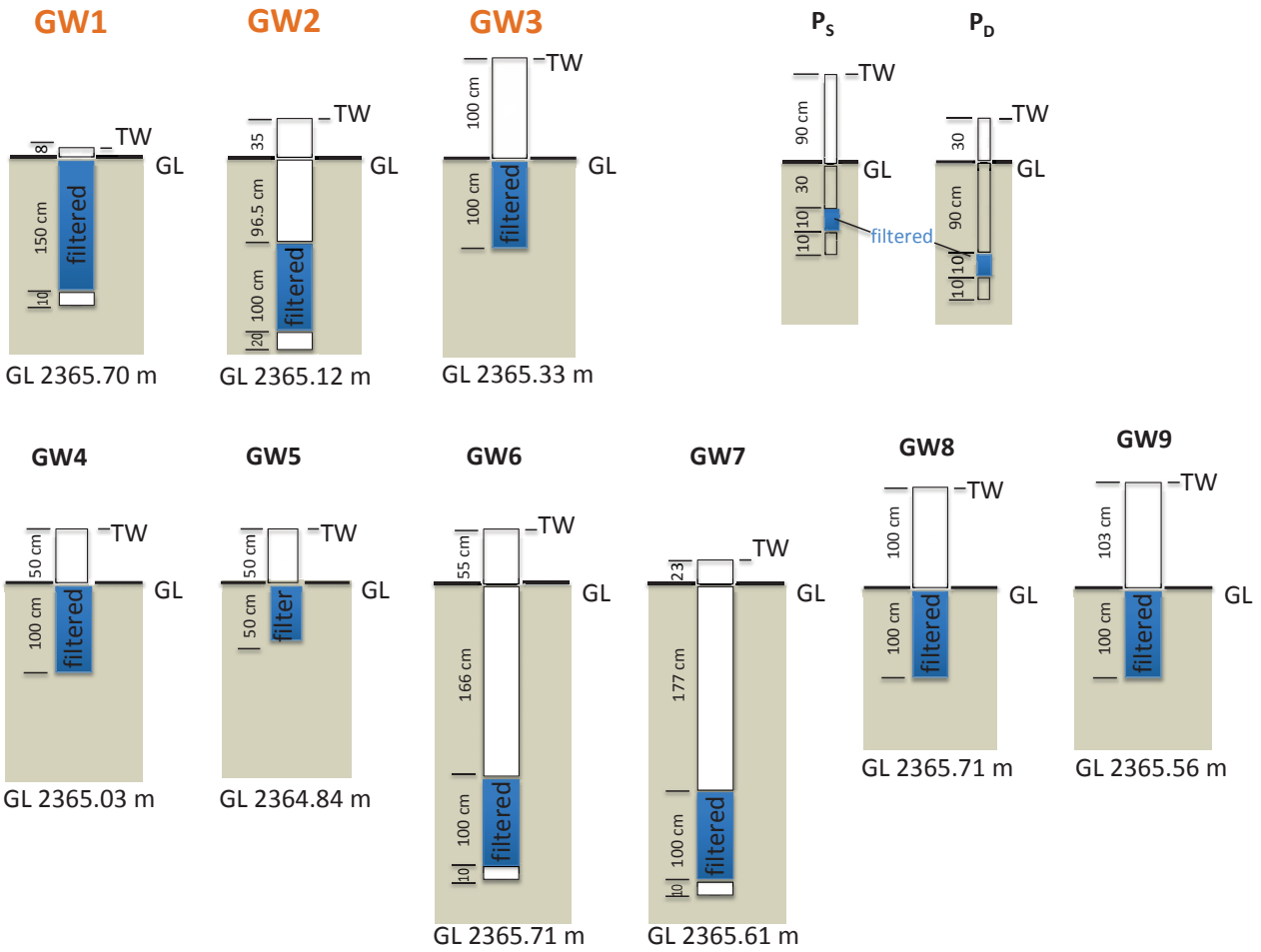

Figure 4.1: Dimension & filtering of the different monitoring wells and mini-piezometers as well as their ground level (GL) in m a.s.l.. GW1, GW2 & GW3 are the major monitoring wells, which have the longest time series (see Tab. 4.1). A shallow (P_S) and a deep (P_D) mini-piezometer is installed next to each of these three monitoring wells, to get the possibility to sample in different depths. Monitoring wells GW4 & GW5 are older ones and no longer used. GW6 & GW8 were installed next to monitoring well GW1, whereas GW7 GW9 were installed closer to the glacial stream (see Fig. 4.2).

Table 4.1: Properties of the different monitoring wells, mini-piezometers & gauge stations. GW1, GW2 & GW3 are the major monitoring wells, which have the longest time series. Sampling campaigns with automated water samplers (ISCO) were only conducted at GW1 & GW2. The other wells were used for snap shot sampling. At each gauging station a water level proportional water sampler (WPW) was installed. The common sampling time was two weeks.

		depth [cm]	**filtering [cm]**	**⌀ [cm]**	**material [cm]**	**GL [m a.s.l.]**	**sensing?**	**sampling?**	**data**
monitoring wells	**GW1**	160	0-150	4	HDPE	2365.70	yes	sampling campaigns	05.06.13-22.10.13; 14.06.14-15.10.14
	GW2	220	100-200	4	steel	2365.05	yes	sampling campaigns	05.06.13-15.10.14
	GW3	100	0-100	4	HDPE	2365.29	yes	snap shot	05.06.13-22.10.13; 14.06.14-15.10.14
	GW4	100	0-100	4	HDPE	2365.03	no	-	-
	GW5	50	0-50	4	HDPE	2364.84	no	-	-
	GW6	276	166-266	4	stainless steel	2365.71	yes	snap shot	16.07.14-15.10.14
	GW7	287	177-277	4	stainless steel	2365.61	yes	snap shot	16.07.14-06.10.14
	GW8	100	0-100	4	HDPE	2365.71	no	snap shot	-
	GW9	100	0-100	4	HDPE	2365.56	yes	snap shot	16.07.14-06.10.14
piezometers	**P_s**	50	30-40	1.6	HDPE	like GW	no	snap shot	-
	P_d	110	90-100	1.6	HDPE	like GW	no	snap shot	-
gauge stations	**Gacial stream**	-	-	-	-	2362.44 (gauge zero)	yes	snap shot/ WPW	10.06.13-15.10.14
	Creek R1	-	-	-	-	2365.07 (gauge zero)	yes	snap shot/ WPW	16.07.14-06.10.14
	Creek R2	-	-	-	-	2366.66 (gauge zero)	yes	snap shot/ WPW	16.07.14-06.10.14

Fig. 4.2 shows the location of the most important instrumentation, such as monitoring wells, meteo station and three gauging stations. To get the isotopic information from precipitation, a rain collector was installed.

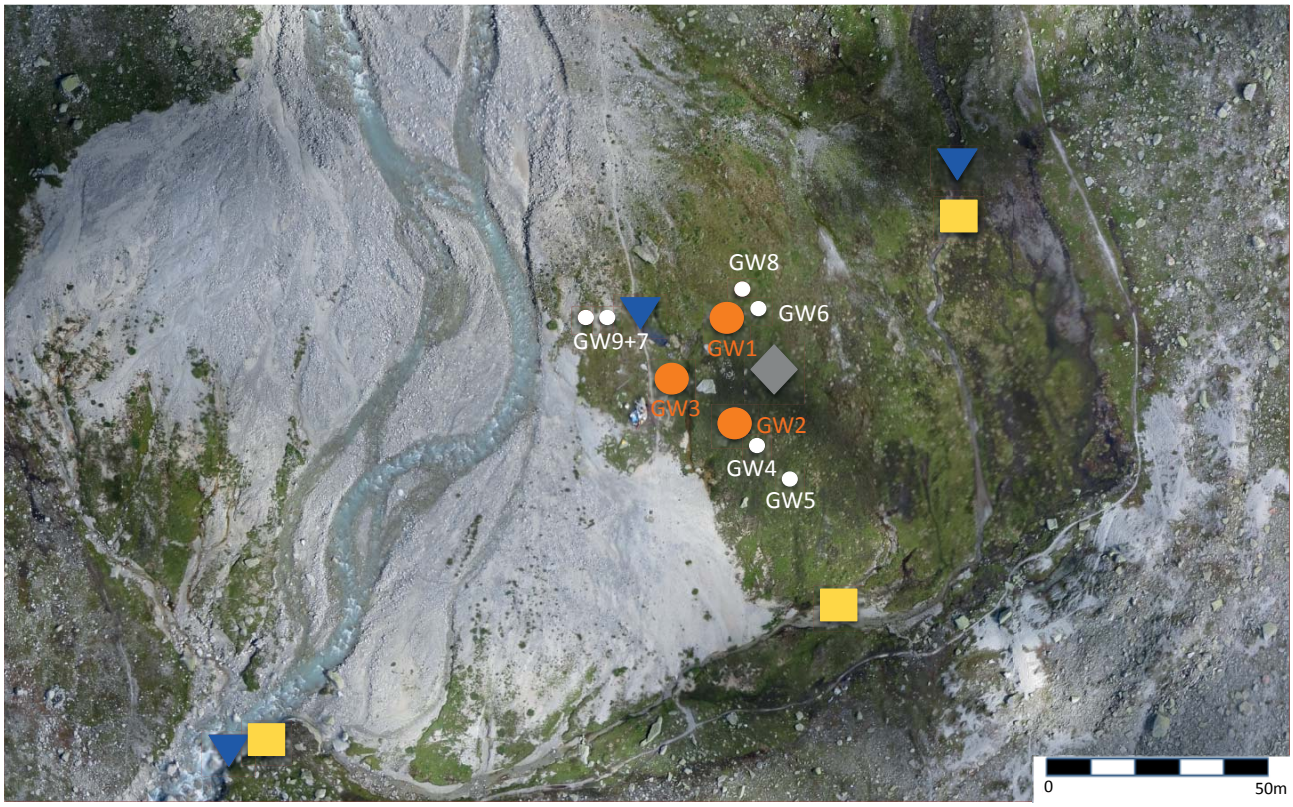

Figure 4.2: Orthophoto (eBee drone, 2014) of test site with marked positions of the different instrumentation; orange & white circles show monitoring wells, blue triangle symbolizes gauging station, grey diamond is the meteo station & the yellow square shows the location of the water-level proportional water samplers (WPW) installed at the creek as well as in the glacial stream.

Since 2008 the *WSL Institute for Snow and Avalanche Research* (SLF) has operated a climate station at this floodplain. In summer 2013 this station was removed, so that the research group from GIUZ installed new meteo station at the same location measuring following parameter: air temperature, precipitation amount, incoming solar radiation, wind speed & direction and the soil moisture. Additionally, the evolution of snow height is recorded based on time-lapse cameras.

4.2.2 Sampling strategy

Due to the online access to the data from the CTD online sensors, specific groundwater sampling campaigns at times of high electrical conductivity (EC), water temperature or hydraulic head (HH) were performed. Therefore, automated water samplers (ISCO 2900) were used. They were programmed to take each 6 h one sample, so that 24 samples were taken over a period of 6 days. Every sampling campaign was conducted with two samplers at two different monitoring wells (GW1 & GW2). Following groundwater recharge phases were tried to sampled: (1) after snowmelt, (2) during intense rainfall and (3) after a possible first snowfall or rain-on-snow event.

Furthermore, manual groundwater, snow and glacial stream samples were collected. Wells were pumped dry using a vacuum pump prior to sampling. In addition to the event & continuous sampling, a snap-shot manual sampling every mid-august was conducted since 2012. Precipitation samples were taken with a rain collector installed on the floodplain, which emptied approximately every two weeks. Additionally, the hut warden of the Albert-Heim hut took a sample if the precipitation was more than 20 mm/d. To measure the isotopic and hydrochemical signal in the glacial stream and the small creeks which goes through the floodplain, a water-level proportional water sampler (WPW) was installed at each gauging station. These samplers use the law of Hagen-Poiseuille, where a capillary (or a valve) controls the sampling aliquot per time by regulating the air flux out of a submersed plastic (HDPE) sampling container (Schneider et al. (in prep.)). This allows us to take water-level proportional samples over a period of 2 weeks. An overview of all the campaigns with an automatic water sampler is presented in Tab. 4.2.

Table 4.2: Sampling campaigns with automated water samplers on monitoring wells GW1 & GW2. Sometimes only a few samples were taken from the automated sampler. Furthermore not all samples have been analysed. The selection of samples was based on fluctuations in hydraulic head or electrical conductivity.

	Start	**End**	**Comments**
2013	30.07.13 18:00	03.08.13 14:00	
	29.08.13 20:00	02.09.13 16:00	
	16.09.13 20:00	20.09.13 16:00	GW1 only 4 samples
	20.09.13 17:00	24.09.13 13:00	
	26.09.13 18:00	02.10.13 14:00	
2014	08.08.14 14:00	12.08.14 10:00	GW1 only 6 samples
	28.08.14 11:00	01.09.14 07:00	
	01.09.14 20:00	05.09.14 16:00	
	06.09.14 14:30	10.09.14 10:30	no samples analysed
	10.09.14 22:30	14.09.14 18:30	no samples analysed
	17.09.14 19:00	23.09.14 13:00	GW1 & GW2 only 8 samples each
	01.10.14 17:00	05.10.14 13:00	no samples analysed

4.2.3 Geophysical survey

A first geophysical survey was conducted in October 2012 to estimate the thickness and spatial extent of the aquifer. Therefore, a *electrical resistivity tomography* (ERT) was used. Two Transects were made with each 100 electrodes using the wenner array with a spacing of 2 m. The transects were orientated in south-north and east-west direction (Fig. 4.3 white lines). The second survey in October 2014 was conducted with 50 electrodes and a spacing of 0.5 m. Two similar aligned transects in east-west direction (Fig. 4.3 black line) were investigated. The smaller spacing provides higher data resolution of the sediments closer to the surface. For this area a layer boundary in the first meter is expected.

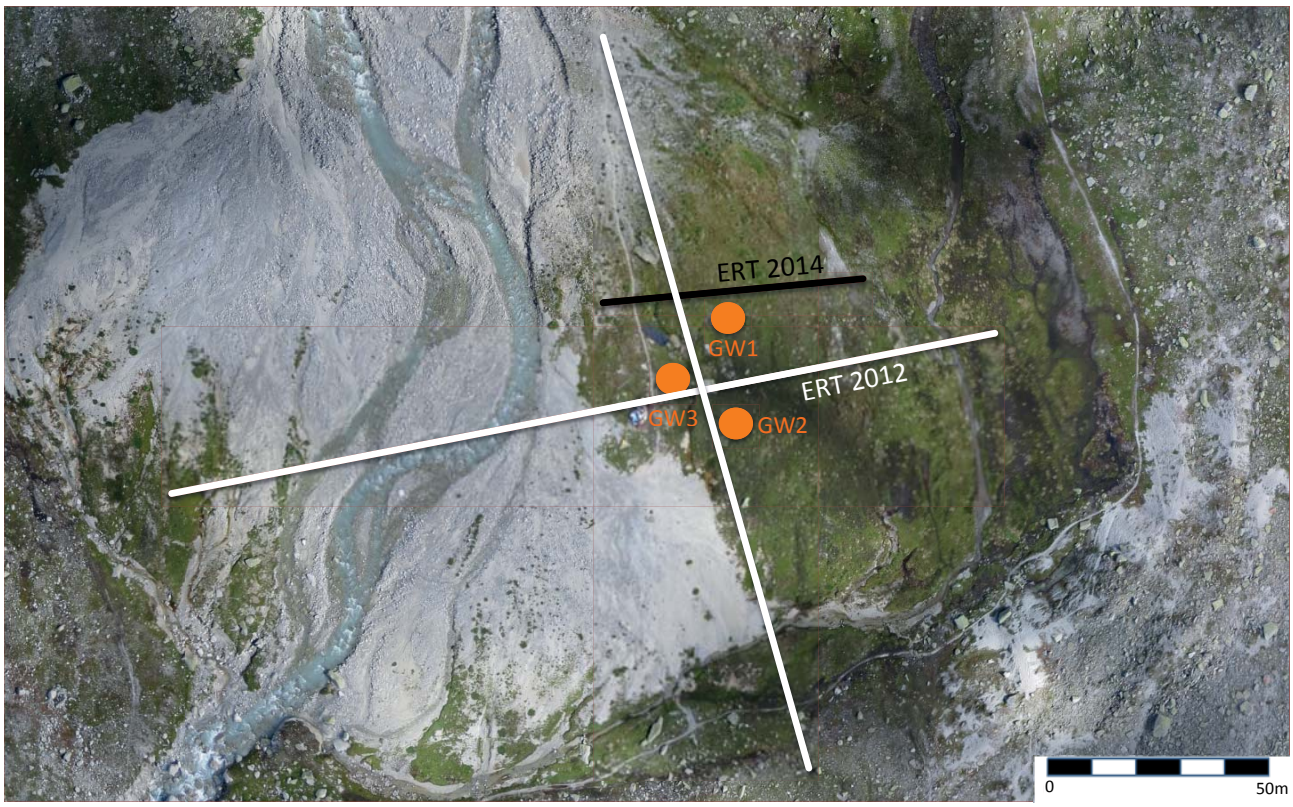

Figure 4.3: Orthophoto (eBee drone, 2014) with marked locations & orientation of ERT transects 2012 (white lines) & 2014 (black line). Two transects (E-W & S-N) were investigated at the ERT 2012, using a wenner array and a spacing of 2 m. In 2014 the ERT was conducted with 2 transects in line (E-W), a spacing of 0.5 m and wenner array. The spacing was chosen smaller, to get a better resolution in the upper zone.

4.2.4 Pumping & slug tests

For investigation of hydraulic conductivity of the aquifer a couple of pump & slug tests as well as infiltration tests with Guelph-Permeameter were conducted. The infiltration tests with Guelph-Permeameter were made in the immediate vicinity of those monitoring wells, where the pump- & slug tests were performed (see Fig. 4.4), to keep it comparable.

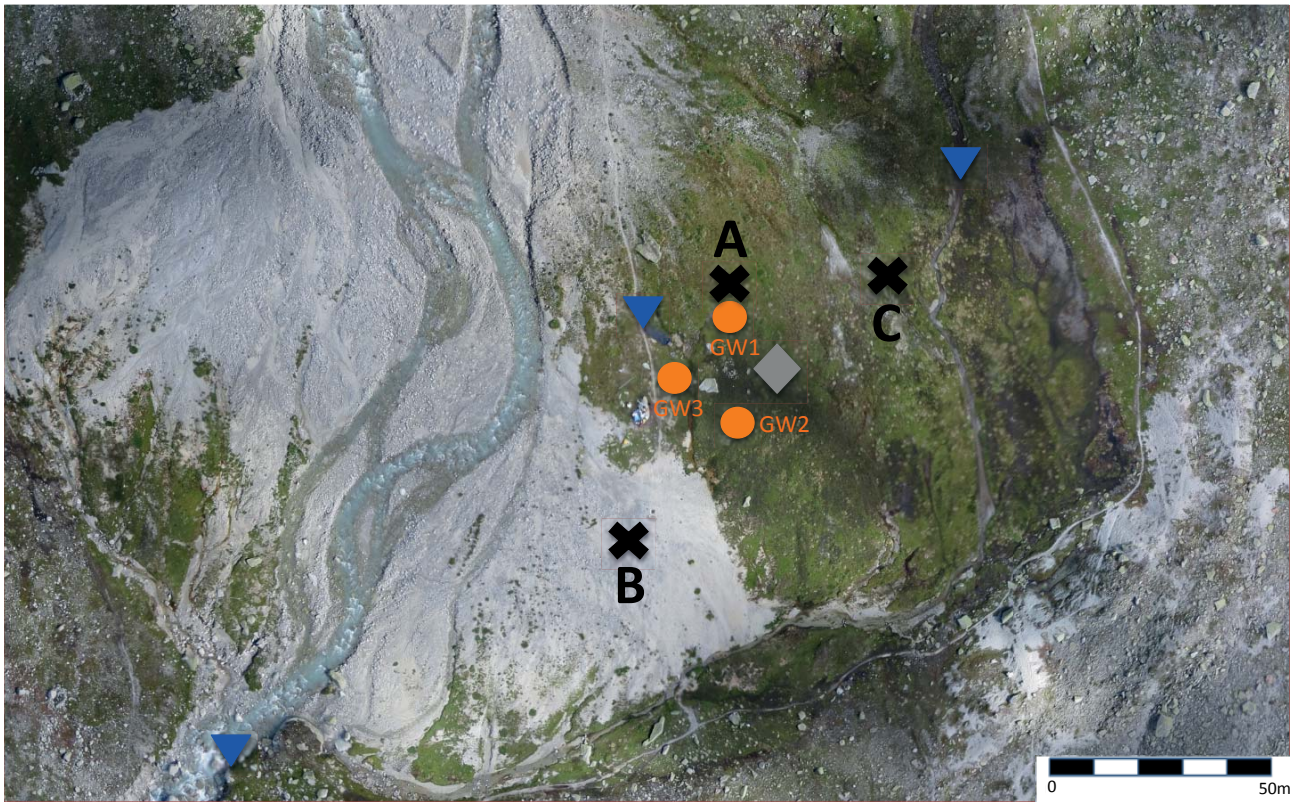

Figure 4.4: Orthophoto (eBee drone, 2014) with marked locations of slug and infiltration test sites (A, B, C). The slug test at site A was performed in monitoring well GW1. For site B & C furthermore wells were installed. The infiltration tests with Guelph-Permeameter were performed in direct vicinity to the slug tests.

Infiltration tests with Guelph-Permeameter

The Guelph-Permeameter (Fig. 4.5) is a constant-head permeameter, based on the principle of Marriotte, for measuring in-situ hydraulic conductivity. It will be measured the steady-state rate of water recharge into an unsaturated soil from a bore hole, in which a constant depth (head) of water is maintained. The Guelph-Permeameter is intended for measurements in the unsaturated zone (Soilmoisture Equipment Corp. 2012). It was also tried to use it for slug tests combined with a self-made double-packer system in the monitoring wells for the saturated zone, but it failed to work fine. It was not possible to get a steady-state rate of water recharge maybe because of a air leakage somewhere in the system. The analysis of the infiltration tests were made with an calculation sheet from Soilmoisture Equipment Corp. (2012).

Figure 4.5: Photo of Guelph-Permeameter (Soilmoisture Equipment Corp. 2012)

Slug tests

Slug test are performed to estimate hydraulic conductivity (K) of aquifers by measuring the recovery of hydraulic head as a function of time after a rapid (instantaneous) change in water level. The change in water level can be achieved by adding (slug test) or removing (bail test) a certain volume of water or solid into the well (Kalbus et al. 2006). In this case, 4 l water were filled abrupt in the monitoring well and the recovery of the hydraulic head was measured. Afterwards, the time series were manually trimmed so that the start represents the highest water table. For slug tests not much equipment is required and they are quick and easy to perform. With this method, it is possible to get a lot of point measurements in short time (Kalbus et al. 2006). Slug tests were analyzed by the method of Bouwer & Rice (1976) and Hvorslev (1951). The method by Bouwer & Rice is based on the Thiem equation.

$$Q = 2 \cdot \pi \cdot K \cdot L_e \cdot \frac{y}{ln(\frac{R_e}{r_w})} \tag{2}$$

Q: volume rate of flow into well $[m^3/s]$
K : hydraulic conductivity of aquifer around well [m/s]
L_e: length of well screen [m]
y: vertical section between water level inside level and static water table outside [m]
R_e: effective radial distance over which y is dissipated [m]
r_w: radial distance of undisturbed portion of aquifer from centerline [m]

where

$$K = \frac{{r_c}^2 \cdot ln(\frac{R_e}{r_w})}{2 \cdot L_e} \cdot \frac{1}{t} \cdot ln \cdot \frac{y_0}{y_t} \tag{3}$$

r_c: radius of the casing [m]
t: Time [s]

with

$$ln(\frac{R_e}{r_w}) = [\frac{1.1}{ln(\frac{L_w}{r_w})} + \frac{C}{\frac{L_e}{r_w}}]^-1 \tag{4}$$

L_W: section of well under water table [m]

Due to the relative small diameter of the monitoring wells, it wasn't possible to abruptly pour all of the water. This problem resulted in a big discrepancy in the analysis by Bouwer & Rice method, because the input volume of water plays a role. This means, that a lot of the water gets lost before the trimmed time series starts. With an adapted water volume, calculated based on water level and diameter of well, the analysis works fine. Because of this discrepancy, K_{sat} was additionally calculated with Hvorslev's method (Eq. 5).

$$K_{sat} = \frac{{r_c}^2 \cdot ln(\frac{L_e}{r_w})}{2 \cdot L_e \cdot t_{37}} \tag{5}$$

K_{sat}: saturated hydraulic conductivity [m/s]
r_c : radius of well casing [m]
L_e: length of well screen [m]
r_w: radius of well screen [m]
t_{37}: time, when water level rises or falls 37% of initial HH [s]

Pumping tests

Fig. 4.6 (a) shows the self-made double-packer system. Its a polypropylene pipe with two pieces of a bike inner tube (each with a valve). These tube pieces are fitted on the pipe and are air-sealed with shrinking tube at both ends. Both valve cores are removed and placed on the end of a pressure tube, in order to open and close the system. Once this is done, two packers can be filled separately with air through the pressure tube. With this double-packer system it is possible to investigate specific layers of the aquifer with a height of 20 cm.

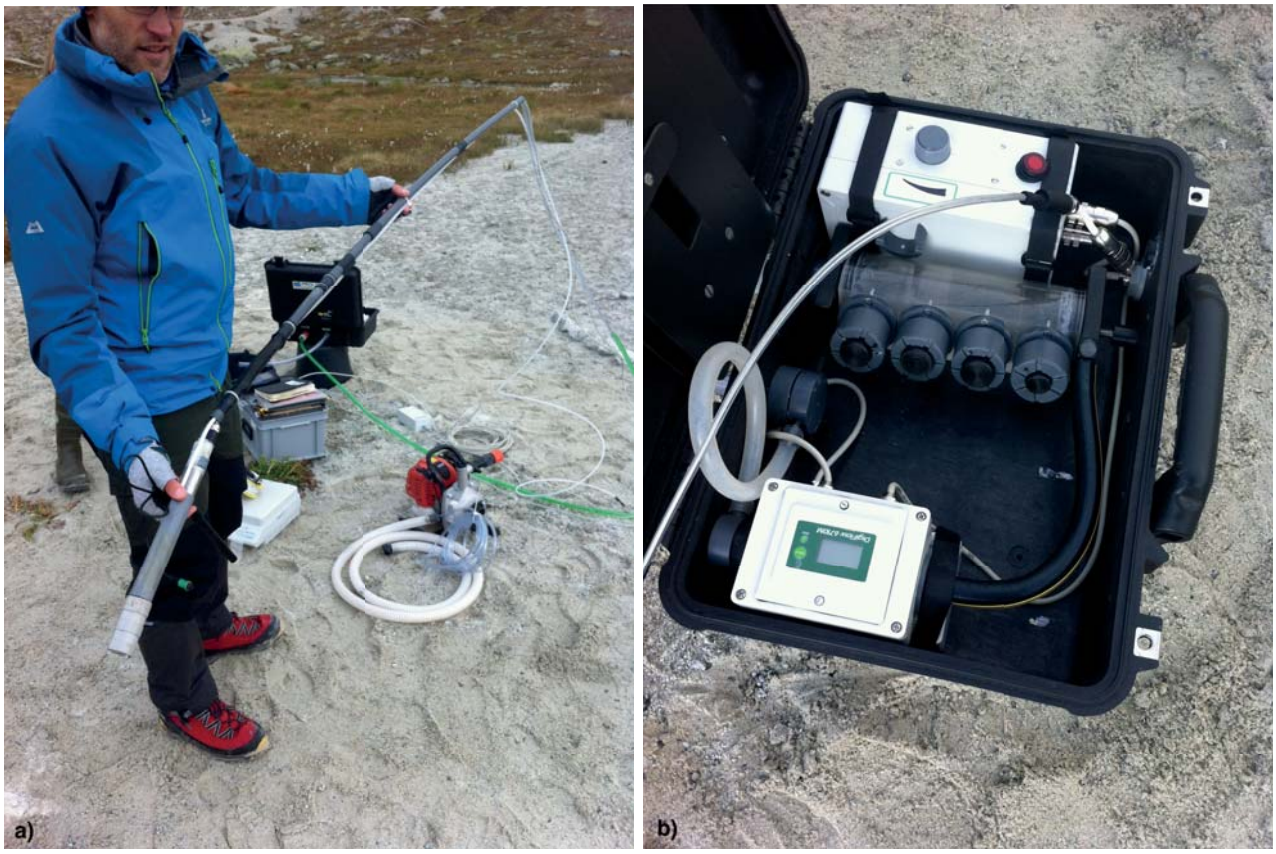

Figure 4.6: (a) Self-made double packer system with attached pressure sensor and electrical water pump. (b) Prototype of pumping devices.

Fig. 4.6 (b) shows a prototype of a pumping device. It was developed from the company *Prologs*. The principle is, that water is pumped from an external pump through a measuring chamber, where it is possible to install four different sensors, and then through a flow meter. An integrated data logger for the sensors and the flow meter could be connected via Bluetooth to a computer for transmitting the online data. It is possible to connect additional sensors to the data logger, which can be installed in the monitoring wells during the pump tests. The design is very compact, because it could all be stowed in a 45 x 32 x 17 cm hard plastic case with a total weight < 10 kg. Thus, it is ideally suited for measurements in remote areas.

4.2.5 Estimation of storage capacity for the alluvial aquifer

The same method like Clow et al. (2003) and Hood & Hayashi (2015) (Eq. 6) was used for estimating the storage capacity of the aquifer and the changes during the winter outflow.

$$V_s = A \cdot d \cdot n_d \tag{6}$$

V_s: storage capacity of aquifer $[m^3]$
A : areal extent $[m^2]$
d: depth of aquifer $[m]$
n_d: porosity [-]

The aquifer should be divided in an active and a passive part, since not the entire aquifer could drain into the glacial stream due to different absolute elevations. As active aquifer, the part which drained to the glacial stream was defined, thus above gauge zero at the catchment outlet (2362.44 m a.s.l.). Only groundwater from the active part of the aquifer can contribute to the runoff of the glacial stream, following this definition. The passive aquifer is accordingly below 2362.44 m a.s.l. Deeper groundwater may be able to percolate through fissures in fractured crystalline rock.

4.3 Laboratory methods

4.3.1 Silica analysis

The silica analysis was performed using photometric measurements, according to the method described in DIN38405-D21 (1990). Therefore, a spectrometer (*Specord 40* from *Analytik-Jena*) was used. Samples for silica analysis are stored in low density polyethylene bottles, because glass bottles could falsify the results due to possible dilution of silicon from the glass. Before analysis, the samples were filtered with 0.45 μm cellulose-acetate filters, because suspended solids could impact the measurement. To minimize potential errors, measuring was made twice. The results were averaged. If the difference was bigger than 0.01 mg/L, the sample were measured a second time. The principle of silica measurement is based on the fact that the dissolved silicic acid by the addition of ascorbic acid and ammonium molybdate tetrahydrate forms a blue complex, which can be measured by a spectrometer. Because phosphorous also affect to build this complex, these ions have to be masked selective by adding tartaric acid.

$$H_4SiO_4 + 12H_2MoO_4(polymer) \rightarrow H_4Si(MO_3O_{10})_4 + 12H_2O \tag{7}$$

The formed color complex has an extinction maximum in the range of 815 nm. The calibration of the photometer was made with 6 standards in range from 0.2 to 2 mg/L, as well as a "blind"-standard with 0 mg/L. A new calibration was made for each measuring series. The determination coefficient r^2 for each calibration was $r^2 = 1.0$.

4.3.2 Isotope analysis

Samples for isotope analysis were taken separately in 20 ml glass bottles. To prevent evaporation, which would influence the result, it is essential to keep the samples airproof (Kendall & McDonnell 1998). The samples were filtered with 0.45 μm PTFE filters and pipetted in 1.5 ml vials for the laser spectrometer. They were stored in the fridge at 5 - 7 °C until analysis. The analysis was conducted with a laser spectrometer *Picarro L2130-i* (cavity rind-down spectroscopy). As reference standard was used an inhouse standard, which is calibrated against VSMOV. The laser spectrometer measures the isotope ratio in relation to a given standard, because it's much easier and more precise to measure the relative or absolute difference between two samples than their absolute ^{2}H or ^{18}O content (Dansgaard 1964).

$$\delta = \frac{R_{sample} - R_{standard}}{R_{standard}} \cdot 10^3 \text{ ‰} \tag{8}$$

R_{sample}: isotopic ratio of the sample
$R_{standard}$: isotopic ratio of the given standard
R_D or $R_{^{18}O}$: D or ^{18}O - isotopic ratio of the sample

$$R_{^{18}O} = \frac{[H_2{}^{18}O]}{[H_2{}^{16}O]} \tag{9}$$

$$R_D = \frac{[HD^{16}O]}{[H_2{}^{16}O]} \tag{10}$$

The VSMOW - values are:

$$R_{^{18}O} = 2.0052 \cdot 10^{-3} \tag{11}$$

$$R_{^{2}H} = 1.5575 \cdot 10^{-4} \tag{12}$$

(Kendall & McDonnell 1998)

The analytical uncertainty for this method and devices of ^{2}H and ^{18}O measurements is ± 0.6 ‰ and ± 0.16 ‰, respectively. The error for DE results from the errors of the two isotopes. According to Froehlich et al. (2002), the error is calculated as follows:

$$u(d) = \sqrt{(u\delta^2 H)^2 + 8 \cdot (u\delta^{18}O)^2} \sim \pm\ 0.75 \text{ ‰} \tag{13}$$

4.3.3 Ion chromatography

The major cations and anions were measured using ion chromatography (761 Compact IC, Metrohm) that is hosted at the lab of environmental science at the ETH Zürich. The Precision is about $<$ 2 % for concentrations of 1 - 200 mg/L. Water samples for ion chromatography were filtered with 0.45 μm Nylon-filter and stored in polyethylene bottles. Nylon-filters were used due to previous test measurements, where these filters show the lowest contamination. For the analysis of the cations it is necessary to acidify the samples with HCl, for example. Thus, it is necessary to take a second volume from the sample, because HCl would falsify the result for anion Cl^-. This means, that normally every sample would be measured twice. However, only measurements with acidified samples were conducted, because the sample volume is sometimes minimal and the fact that the alternative would have been twice as expensive. Consequently, the results for Cl^- could not be used. One soil sample (taken on 20.02.2015) from the upper soil layer in the near of monitoring well GW1 was also analysed. Three different preparations have been analysed. For the first two preparations 50 g soil was mixed with 100 ml deionised water, shaken for 3 h and afterwards filtered. Afterwards a third preparation was made with 50 g soil and 100 ml deionised water.

5 Results

5.1 Time series of hydraulic head, groundwater temperature and electrical conductivity

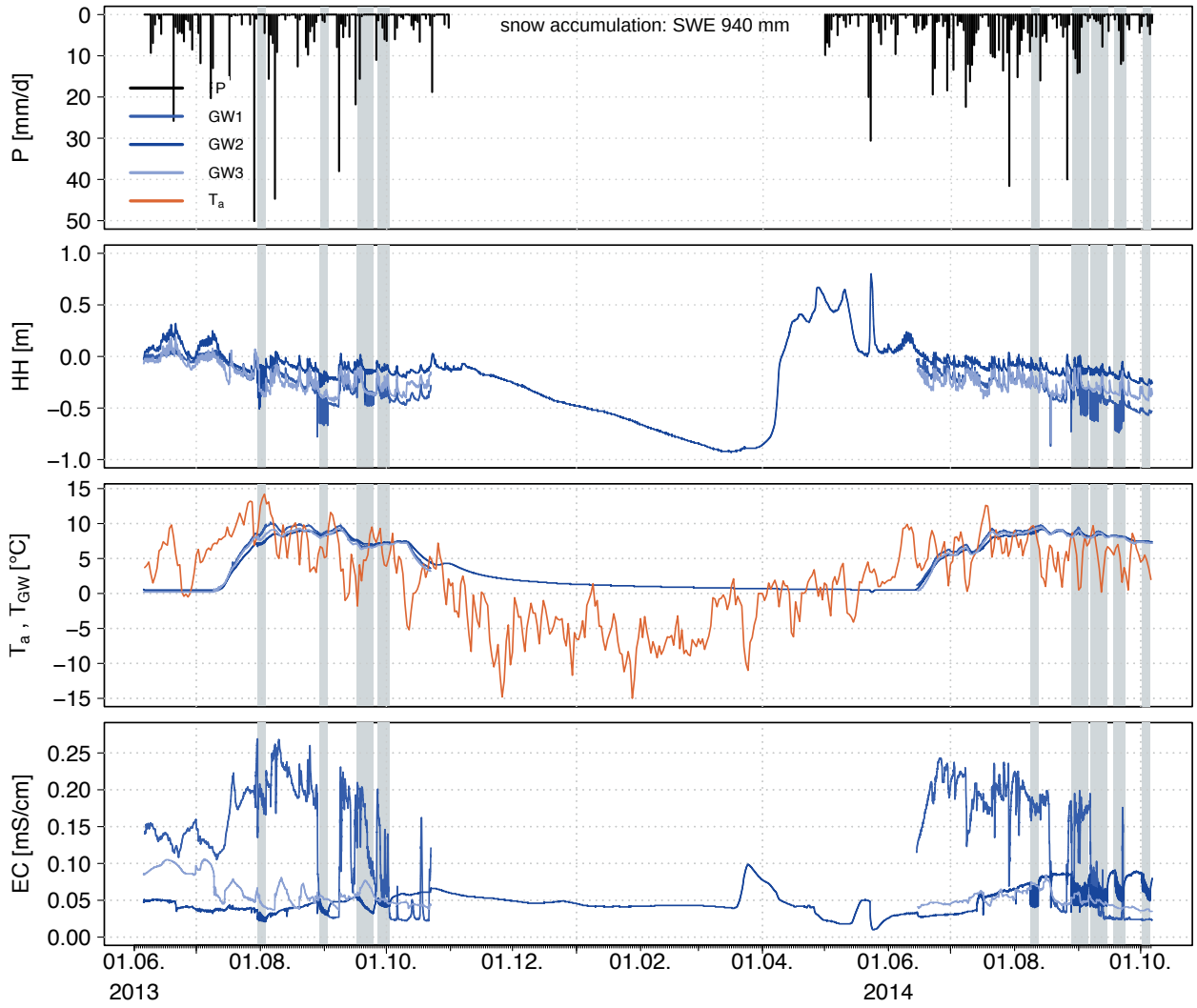

Figure 5.1: Mean daily precipitation (P) & mean daily air temperature (T_a); Hydraulic head (HH, depth to groundwater), groundwater temperature (T_{GW}) and electrical conductivity (EC) at 3 different monitoring wells GW1 - 3; GW1 is 1.5 m fully filtered (GL = 2365.7 m a.s.l.), GW2 partly filtered from 1 to 2 m depth (GL = 2365.05 m a.s.l.) & GW3 is 1 m fully filtered (GL = 2365.3 m a.s.l.) see Fig. 4.1; Sampling campaigns at GW1 & GW2 with automated water samplers are highlighted in grey; HH, T_{GW} and EC are measured in 15 min time steps with CTD online Sensors from HT.

Fig. 5.1 shows the time series of hydraulic head (HH), groundwater temperature (T_{GW}) and electrical conductivity (EC) for three different monitoring wells (GW1-3) at the test site. The daily precipitation and the mean daily air temperature are also shown. The only sensor that was installed during the winter was in monitoring well GW2, because it was not certain if the sensors would freeze or be destroyed. The time series started on 6 June 2013 and went until 15 October 2014. The monitoring wells have different screenings and ground levels (see Fig. 4.1). The unequal ground levels causes a little offset on HH. In the time series of HH and T_{GW} there is no significant difference visible between the three monitoring wells. During the summer month, the HH fluctuates strongly.

Most of them are coincided with precipitation events. During winter, a constant decrease in HH as well as in T_{GW} for GW2 were detected. EC shows no significant changes during the winter except one abrupt increase from 0.05 to 0.10 mS/cm (24.03.2014) followed by slow decrease up to 0.025 mS/cm. This peak in EC accompanied a very moderate increase in HH. Prior to this, the mean daily air temperature rises temporary up to about 2.5 °C. At the beginning of April, the HH increases clearly from about -0.8 m to +0.6 m. A positive HH means that the groundwater extends into the snow cover, which can be seen in Fig. 5.2.

Figure 5.2: The picture shows meltwater standing up in the snow cover during snowmelt 2012 (24.05.12). The hydraulic head of the resulting meltwater lake was 1.8 m above ground level in a snow cover of 2 m depth. Similar conditions could be assumed from our data for the snow melt periods 2013 & 2014. (Schneider, 2012)

This picture was made during times of snowmelt in 2012. According to the time series, it could be assumed that the same happened in 2013 and 2014. On 23.05.14 an abrupt increase in HH from 0 m to 0.75 m occurred and was accompanied by a small but clearly decrease in T_{GW}. These changes are induced by a rain on snow (ROS) event with 30 mm/d. At middle of June 2014 the T_{GW} increase again after the winter time. In 2013 as well as in 2014 the T_{GW} reaches its maximum of about 10 °C, which is surprisingly high at 2300 m a.s.l.. Another interesting outcome is the different course of EC for the three wells. While GW2 & GW3 show relative moderate courses of EC, GW1 shows great abrupt leaps from 0.25 to 0.025 mS/cm. The range of mean daily air temperature extend from ~ -15 to $\sim +14$ °C.

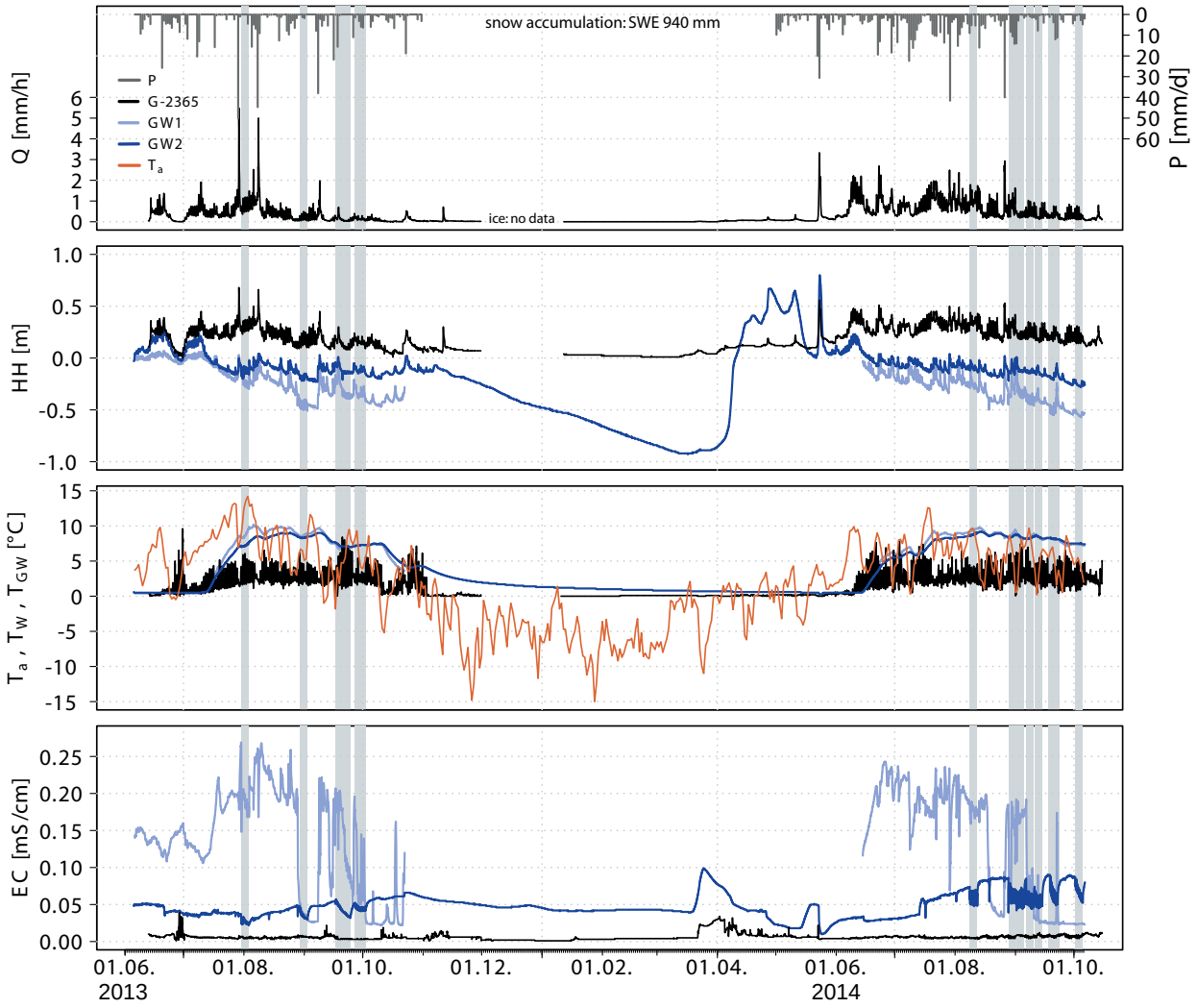

Figure 5.3: Mean daily precipitation (P) & mean daily air temperature (T_a), runoff from glacial stream [mm/d], hydraulic head (HH, depth to groundwater), groundwater temperature (T_{GW}) and electrical conductivity (EC) from 2 different monitoring wells as well as hydraulic head (water level above gauge zero), water temperature (T_W) and electrical conductivity (EC) from glacial stream; HH, T_{GW} and EC measured in 15 min time steps at monitoring wells GW1 & GW2; GW1 is 1.5 m fully filtered (GL = 2365.7 m a.s.l.) & GW2 partly filtered from 1 to 2 m depth (GL = 2365.05 m a.s.l.) see Fig. 4.1; Sampling campaigns with automated water samplers are highlighted in grey; HH, T_W and EC measured in 5 min time steps at glacial stream; data from glacial stream and monitoring wells are aggregated to hourly values; runoff is calculated by p/q - ratio, validated for medium and high flows with salt and uranin dilution; not validated for low flows.

Fig. 5.3 illustrates the course of HH, T_W and EC for the glacial stream as well as HH, T_{GW} and EC for Monitoring wells GW1 & GW2. The figure also shows daily precipitation, runoff from glacial stream [mm/d] and the mean daily air temperature. Attention should be paid at HH of groundwater and glacial stream. The HH from glacial stream refers to the zero point of gauge (2362.44 m a.s.l.), whereas HH from groundwater refers to local terrain (GW1 = 2365.7 m a.s.l.; GW2 = 2365.05 m a.s.l.). They can be compared when using absolute values to swiss altitude reference. Unfortunately, the sensor which was installed in the glacial stream froze during winter time. That is the reason for a gap in time series of HH as well as T_W. The course of HH from glacial stream for summer time shows the same performance as the groundwater, both accompany precipitation.

As anticipated, the EC from glacial stream is throughout lower, than those from groundwater. Even the behavior of the EC curve differs, unlike the behavior of HH. Only at the end of March 2014 was a signal in EC of the glacial stream and GW2 detectable.

5.2 Concentration of major ions in groundwater and glacial stream samples

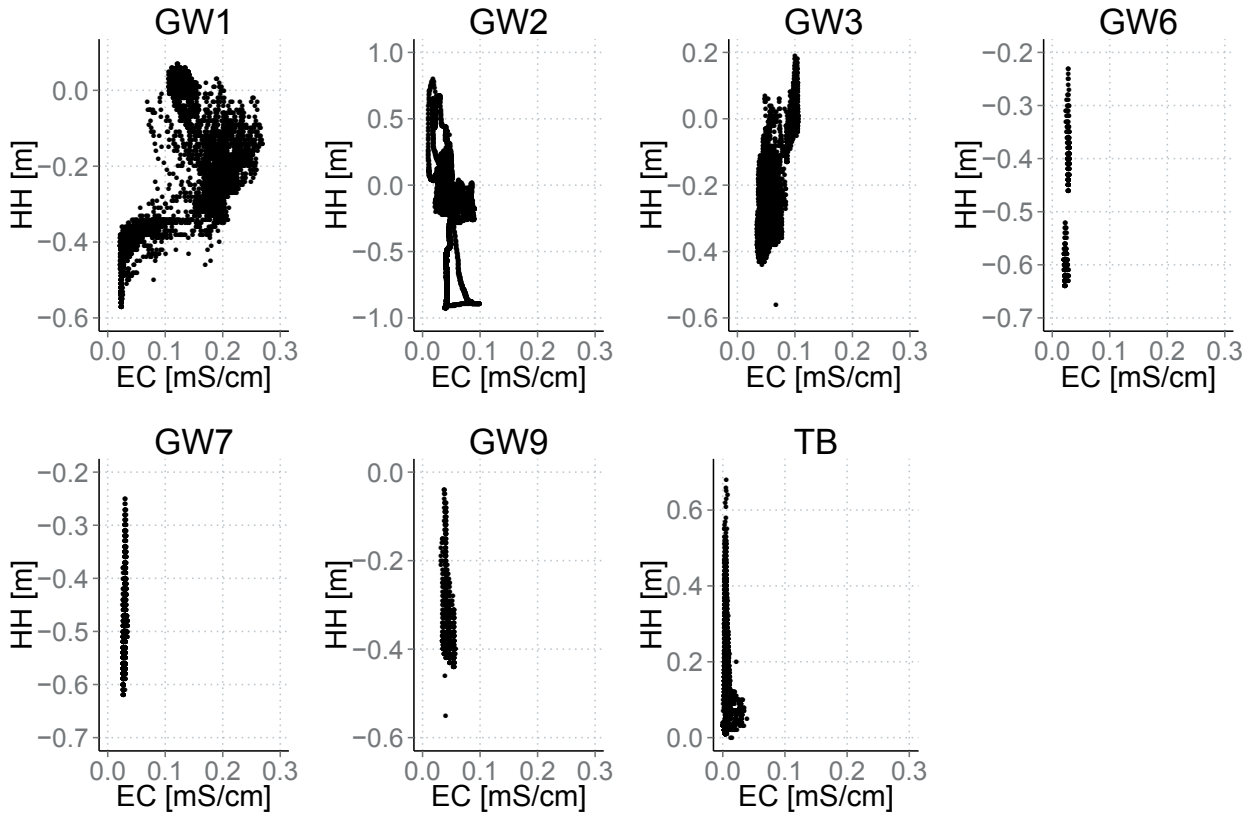

Figure 5.4: Correlation between hydraulic head (HH) and electrical conductivity (EC) at the groundwater wells and the glacial stream based on hourly data. Note that the y-scales differs. The plots show that the variation in EC as well as the correlation between HH and EC is highest for monitoring well GW1. GW6, GW7 & GW9 have only a short time series (see Tab. 4.1), resulting in less data. The different filtering and ground levels off all monitoring wells can be found in Fig. 4.1.

Fig. 5.4 illustrates the correlation between EC and HH. It is evident that at monitoring well GW1 the range of EC is highest. The small range of EC at HH below -0.4 m is interesting. When the groundwater level rises above this height, a clear rise in EC as well as in its range is observable. The data from monitoring wells GW6, GW7 & GW9 show very small variation in EC even if the time series from those wells is only about 2 month. These wells are filtered in a depth of about 2 - 3 m (see Fig. 4.1).

To identify the source of this rise in EC, selected samples were analysed on their concentration of major ions using ion chromatography (IC). The results for some major ions are represented in Fig. 5.5 for samples from monitoring well GW1 (GL 2365.70 m a.s.l.; filtered 0 - 150 cm depth) and in Fig. 5.6 for monitoring well GW2 (GL 2365.06 m a.s.l.; filtered 100 - 200 cm depth). There is a clear correlation between EC and the ions Potassium, Calcium & Magnesium for the samples from GW1 (Fig. 5.5). The other ions don't show a correlation with EC. The plot from Flouride is banded, which is the result of the very low concentration near the detection limit. The resolution is 0.01 mg/L. The same can be noticed for the Flouride concentration of GW2 (Fig. 5.6). For well GW2 (Fig. 5.6) no such clear correlation for the ions and the EC is detectable, whereas the range of EC for GW2 is only a third of that from GW1. Striking are the concentrations of sulphate. While samples from 2013 have concentrations that range from 1.1 up to 1.3 mg/L, samples from 2014 have lower concentrations, ranging from 0.7 up to 0.9 mg/L. Even the EC can be divided in two areas, which means, that the EC in GW2 during sample times from 2013 is throughout smaller than those from 2014.

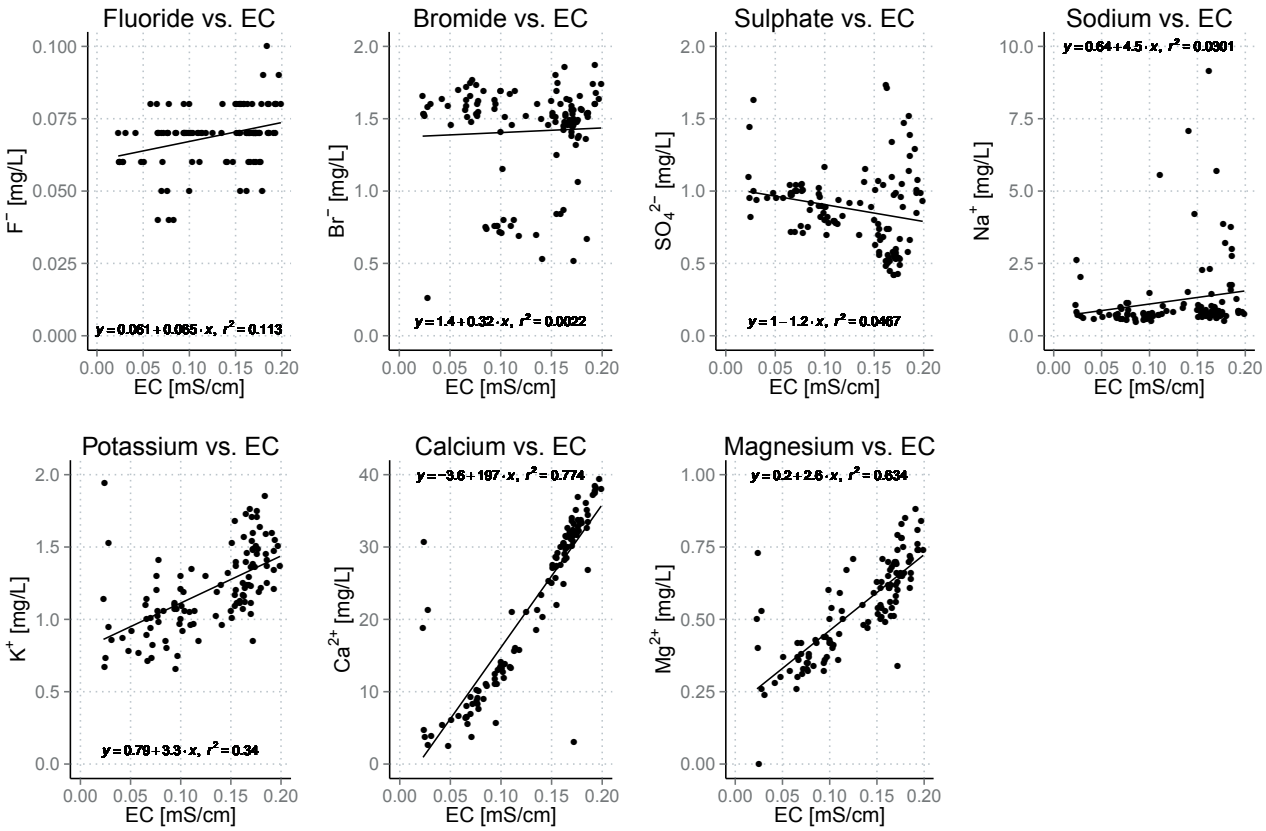

Figure 5.5: Correlation between electrical conductivity (EC) and the concentration of different major ions at groundwater well GW1 (1.5 m fully filtered; GL = 2365.7 m a.s.l.). This monitoring well shows the highest range in EC (see Fig. 5.4). The ions K^+, Ca^{2+} & Mg^{2+} show a clear correlation in their concentrations with the measured EC for the monitoring well GW1 ($n_{samples} = 151$).

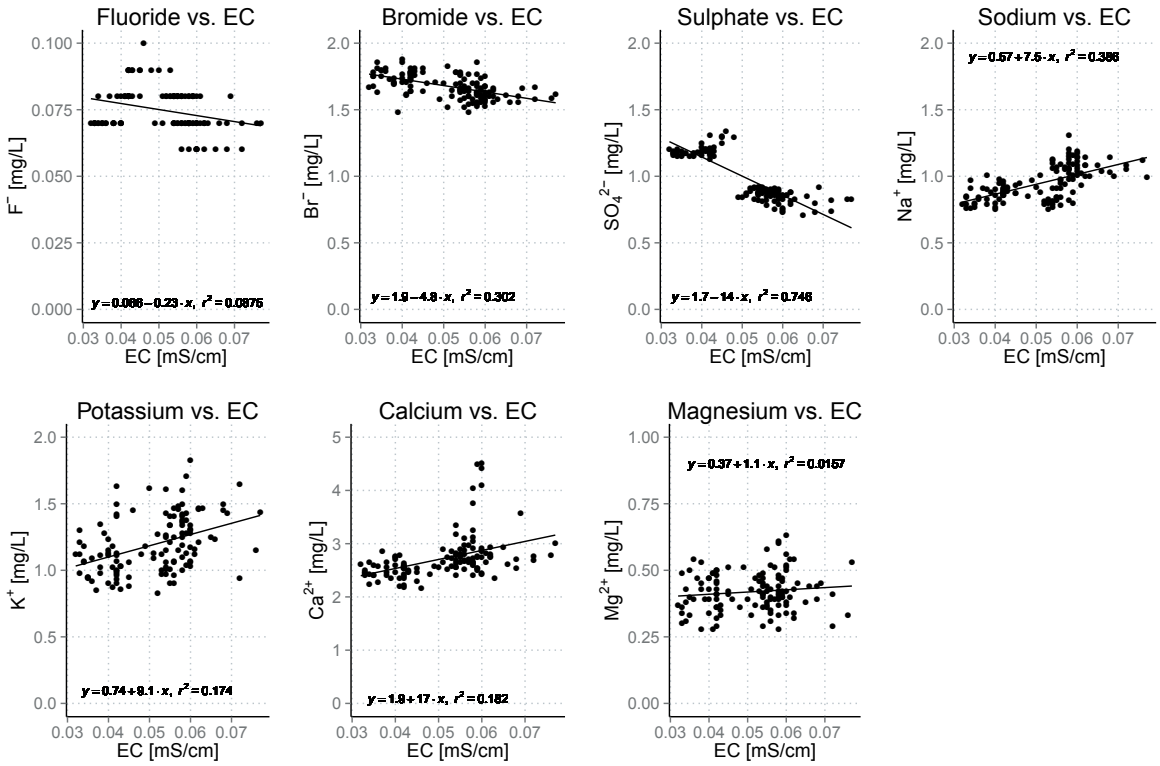

Figure 5.6: Correlation between electrical conductivity (EC) and the concentration of different major ions at groundwater well GW2 (partly filtered from 1 to 2 m depth (GL = 2365.05 m a.s.l.). GW2 has the longest time series and was measured also during winter (see Tab. 4.1). Despite to monitoring well GW1 (Fig. 5.5) there is no significant correlation between EC and the major ions detectable ($n_{samples} = 160$).

The results from IC for the soil sample are presented in Tab. 5.1. The first two preparations show enriched values for K^+ and Cl^-, due to contamination with KCL from the pH measuring device, since KCl is the stock solution for the pH probe. Afterwards a third preparation was made with 50 g soil and 50 ml deionised water, where the pH measurement has been omitted. The soil/water ratio was changed due to the low concentrations of the ions. The 1st and the 3rd preparation have been analysed twice. It is striking, that the values for K^+ and Cl^- are substantially less without the pH measurements. It is also interesting, that Ca^{2+} shows lower values for the lower dilution. The most ions show more or less the same concentration no matter which dilution.

Table 5.1: Results from ion chromatography for the soil sample next to monitoring well GW1. Enriched K^+ and Cl^- values due to contamination with KCL (stock solution of pH probe) are highlighted.

soil / water ratio	Na^+	NH_4^+	K^+	Mg^{2+}	Ca^{2+}	Cl^-	NO^{2-}	Br^-	NO^{3-}	SO_4^{2-}
1st Preparation 2:1	1.93	0.2	64.93	0.45	5.59	61.81	0.27	n.a.	2.68	0.36
2nd Preparation 2:1	2.27	n.a.	8.64	0.2	1.08	8.66	0.03	0.02	2.85	0.34
1st Preparation 2:1	2.26	n.a.	67.71	0.4	2.26	65.05	n.a.	0.07	2.75	0.26
3rd Preparation 1:1	2.08	0.1	2.56	0.13	0.34	0.91	0.03	n.a.	2.67	0.54
3rd Preparation 1:1	2.09	0.13	2.72	0.14	0.35	0.91	0.04	0.02	2.65	0.59

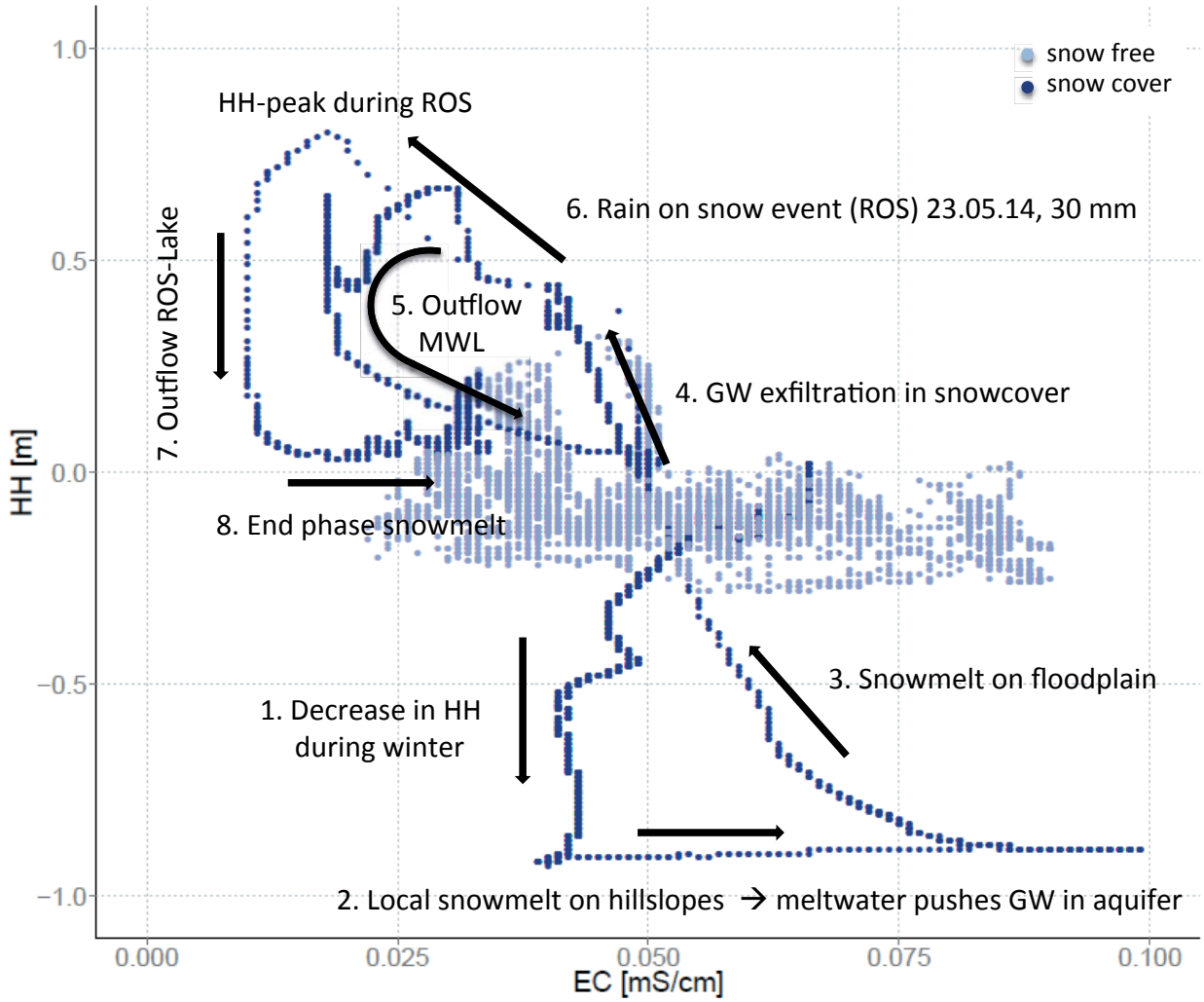

Figure 5.7: Correlation between hydraulic head (HH) and electrical conductivity (EC) at monitoring well GW2. The data series is divided in time of snow cover (15.10.2013 till 15.06.2014) and a snow-free part (summer 2013 & 2014). Processes during winter time, identified with help of time series data (see Fig. 5.1), are named and marked with arrows. MWL = melt water lake.

Fig. 5.7 shows the correlation between HH & EC for GW2, but this time divided in times with snow cover and times without snow. It is striking, that the range in HH is primarily influenced during times with snow cover. The period with snow cover is quiet interesting. Compared with Fig 5.1, different phases and processes during times of snow cover are noticeable. There are also effects of hysteresis visible, which are caused by the rain-on-snow event at 23.05.2014 (left hysteresis loop) and the rise of the groundwater into the snow cover at times of snowmelt (right hysteresis loop). The phases are symbolized in the figure by arrows and numbers. First, there is the outflow of the alluvial aquifer during winter (1) up to a HH of approximately -0.9 m. After that, the EC increases clearly (2) coincided with minimal increase in HH (cf. Fig. 5.1 on 24.03.2014). Then, the period of snowmelt (3) starts. This is characterized by continuous rise in HH and decrease in EC. When the aquifer is filled, groundwater/meltwater exfiltrates into the snow cover (4). After a maximum HH of 0.7 m (5), the exfiltrated water flows out along with an increase in EC.

Phase (4) and (5) form the first hysteresis loop. Since HH is once again near the GL, a second hysteresis loop can be figured out. This is affected by a rain-on-snow event (6) at the end of May 2014. HH reaches its maximum of 0.8 m along with a decrease in EC from 0.05 to 0.02 mS/cm. After that, HH decreases at a constant low EC value (7). Phase (8) shows the end phases of snowmelt with an additional slight increase in HH.

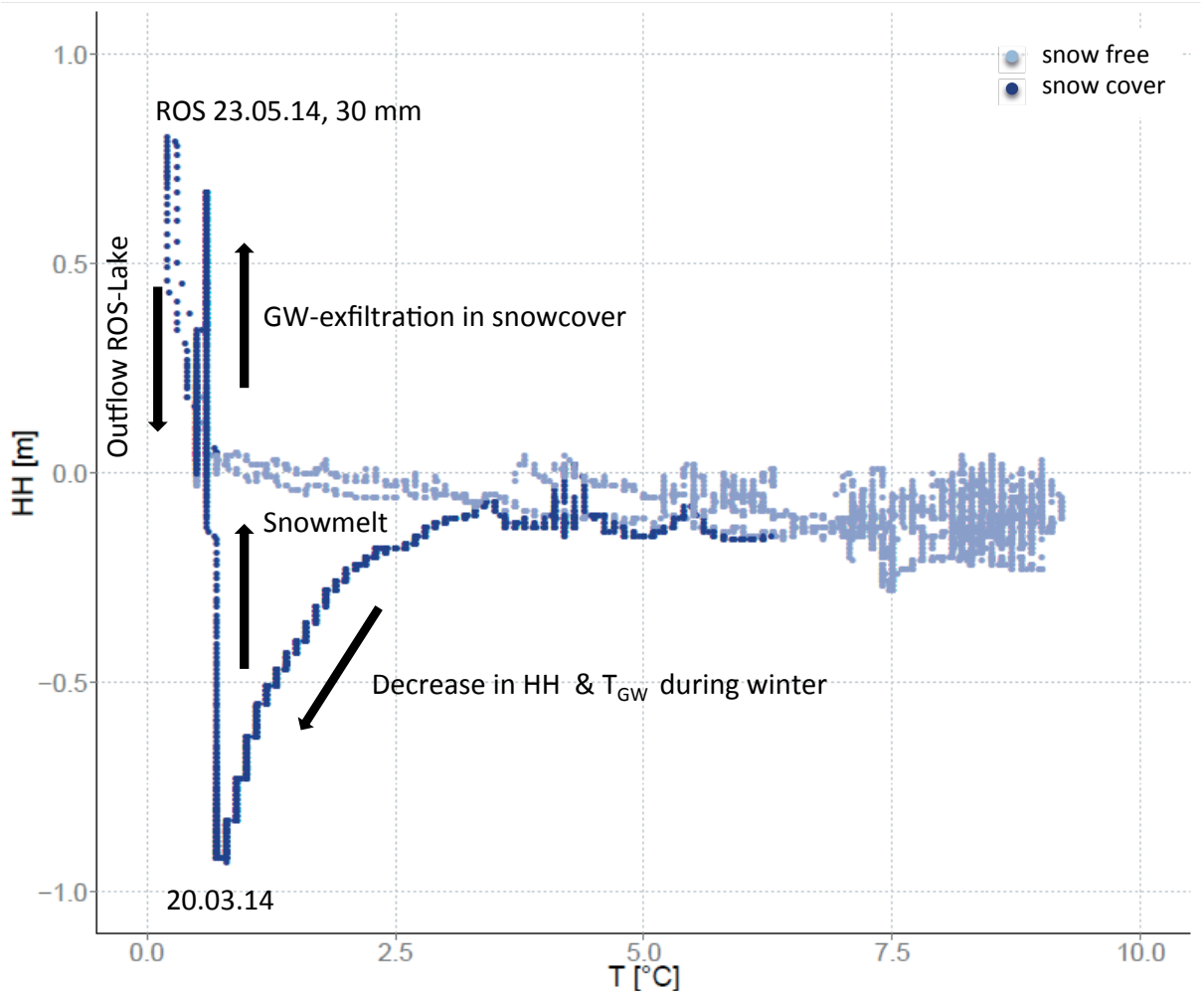

Figure 5.8: Correlation between hydraulic head (HH) and electrical conductivity (EC) at monitoring well GW2. The data series is divided in time of snow cover (15.10.2013 till 15.06.2014) and a snow-free part (summer 2013 & 2014). Major processes for changing HH are named and marked with arrows.

In Fig. 5.8 the correlation between HH and the T_{GW} is shown. Even here some processes can be detected. It is evident, that the T_{GW} are still relative high ($\sim 6.3\,°C$) at the onset of the snow covered period. Compared with Fig. 5.1, the T_{GW} shows a damped decrease during the whole period. This highlights the isolating effect of the snow cover.

5.3 Concentration of dissolved silica

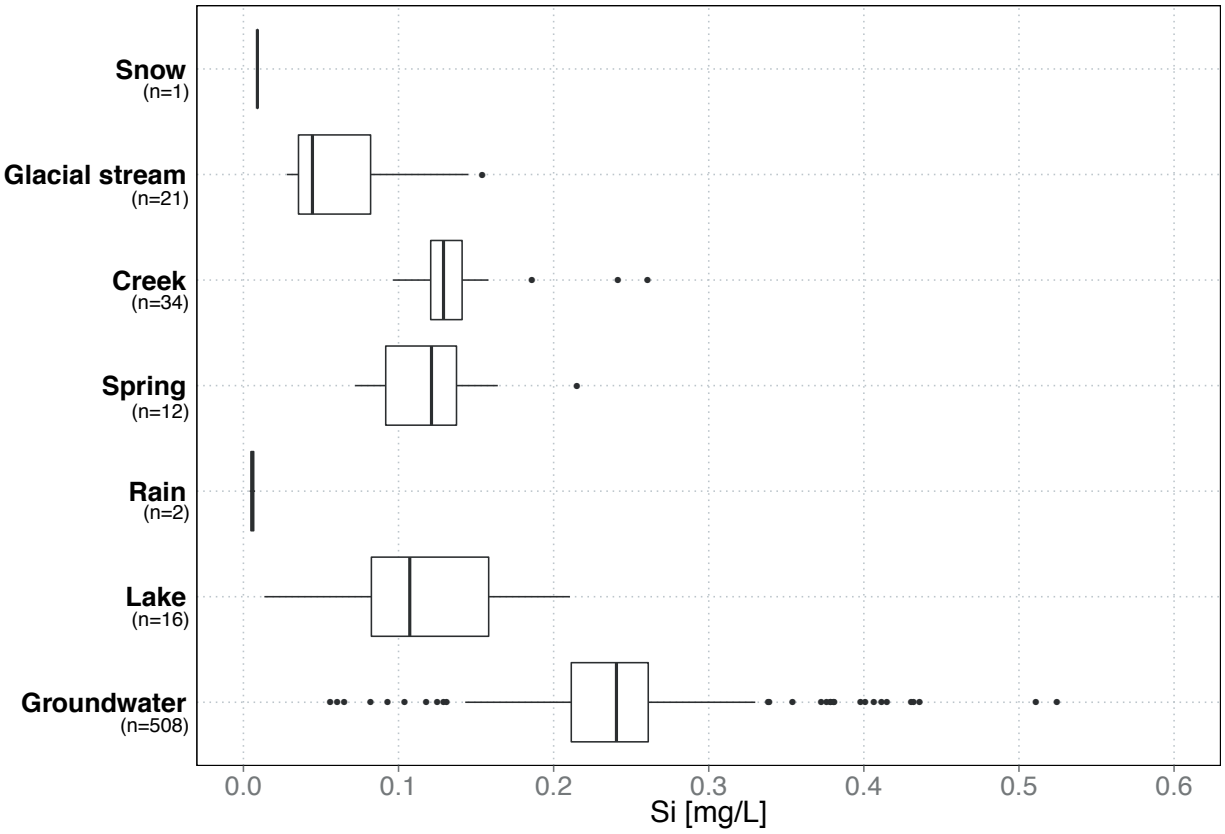

Figure 5.9: Range of silica concentration in samples of glacial stream, creeks, springs, lakes & groundwater. In addition one sample each for snow and precipitation was analyzed, even if concentrations around zero are expected (boxplot: median, box = 1st & 3rd quartiles, wiskers = 1.5 · interquartile range)

Fig. 5.9 shows the range of silica amount in mg/L for different water types. For snow and precipitation only one respectively 2 samples were analysed for silica because there can be expected concentrations around zero for these samples. Groundwater samples have the largest range in silica concentration of $\sim 0.5\,\mathrm{mg/L}$ with values ranging from ~ 0.05 up to $\sim 0.53\,\mathrm{mg/L}$. They also show the highest values compared to the other water types. There are, however, groundwater samples with lower silica values. The samples, which are the lower outliers were taken during a sampling campaign at the end of August 2014 (Fig. 5.10). These samples equally show significantly higher DE values. During the night of 30.08.14 and 01.09.14 it was snowing. The snow was melting the next day. The glacial stream has, aside from winter and summer precipitation, the lowest concentrations of silica. Those values from glacial stream, which are higher than $\sim 0.1\,\mathrm{mg/L}$ are samples that were collected in winter. Springs and their creeks have similar values albeit the median from the creeks is a bit higher.

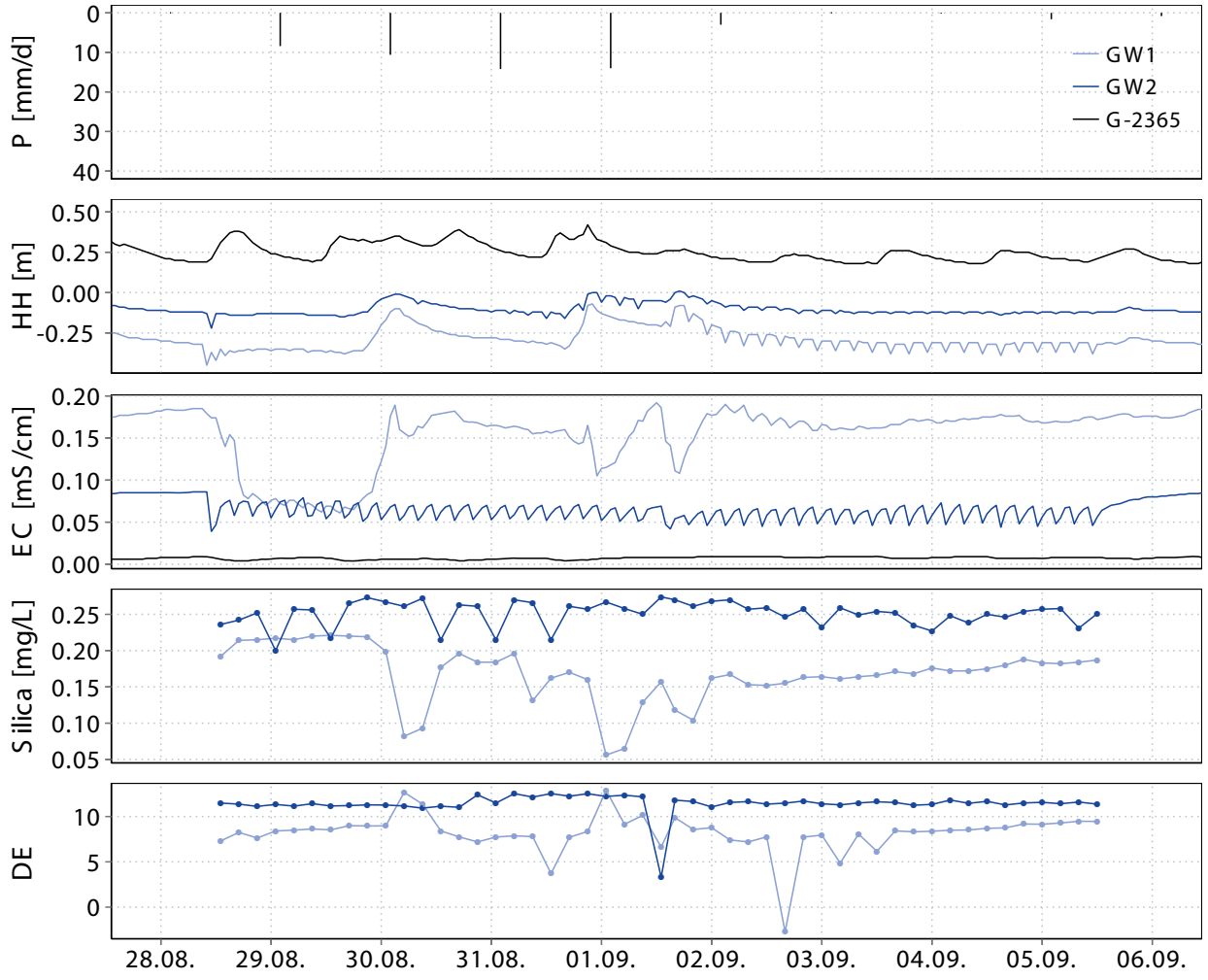

Figure 5.10: Evolution of dissolved silica and DE during sampling campaign from 28.08. - 05.09.14 for monitoring wells GW1 & GW2 as well as HH and EC. Mean daily precipitation (P) is also presented. Sample times are visible by means of fluctuations in EC as well as in HH. Decreases in silica concentration are accompanied by increases in DE.

5.4 Stable isotopes of water

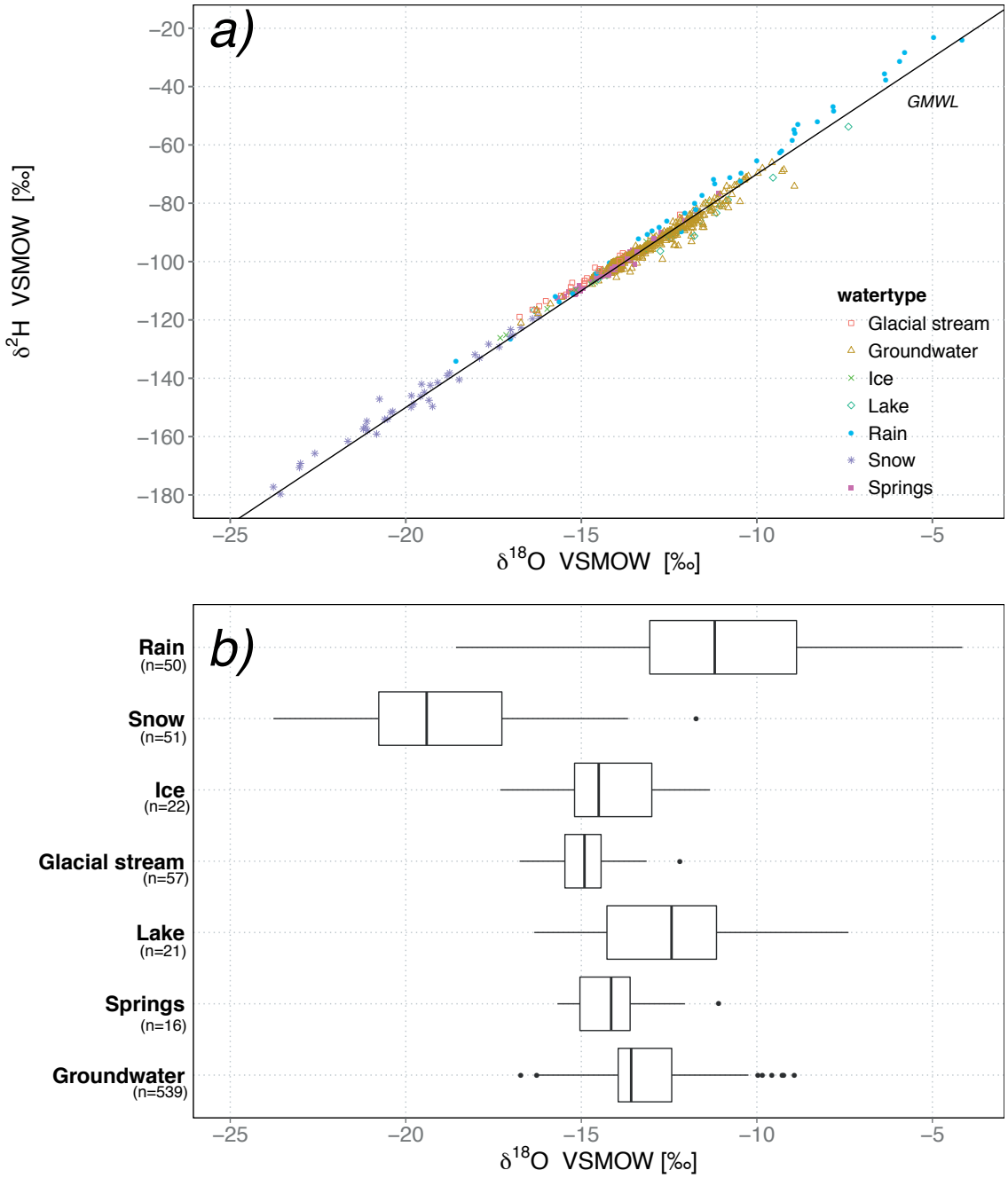

Figure 5.11: (a) Relation between δ^2H and δ^{18}O for different water types including GMWL. (b) Range of δ^{18}O for different water types at the test site (2013 - 2014) (boxplot: median, box = 1st & 3rd quartiles, wiskers = 1.5 · interquartile range)

The results from the stable isotopes are presented in the following section. Fig. 5.11 provides an overview of the isotopic range of samples from the test site from 2013 & 2014. Plot (a) shows the relation between δ^2H and δ^{18}O for different water types including the global meteoric water line (GMWL), defined as $\delta^2\text{H} = 8{\cdot}\delta^{18}\text{O} + 10$. The range in δ^{18}O for each watertype is presented with boxplots in plot (b). There is some evidence that the range for ^{18}O is greatest for summer and winter precipitation.

Together both of these signals indicate large seasonal variations in precipitation of $\sim 20\,‰$ with ^{18}O values ranging from $\sim -4\,‰$ during the summer, down to $\sim -24\,‰$ during winter months. ^{18}O values from the other water types lie approximately in the middle of summer and winter precipitation. Fig. 5.12 (a) shows the relation between $\delta^{18}O$ and the deuterium excess (DE). The range of DE for each watertype is also presented with boxplots (b).

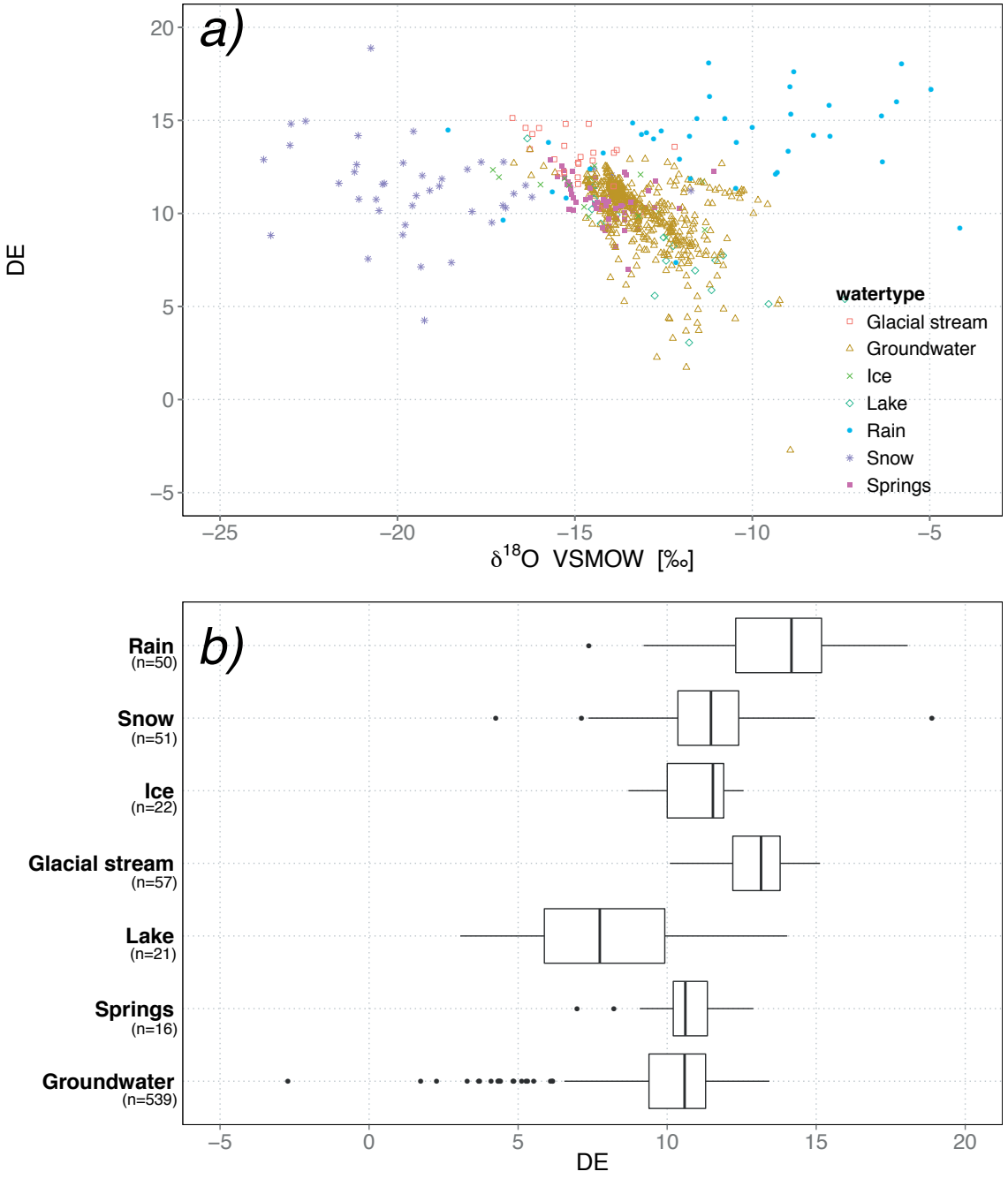

Figure 5.12: (a) Relation between DE and $\delta^{18}O$ for different water types. (b) Range of DE for different water types at the test site (2013 - 2014) (boxplot: median, box = 1st & 3rd quartiles, wiskers = 1.5 · interquartile range).

Due to the high number of samples, these plots are broken down according to the different water types (Fig. 5.13 & 5.14).

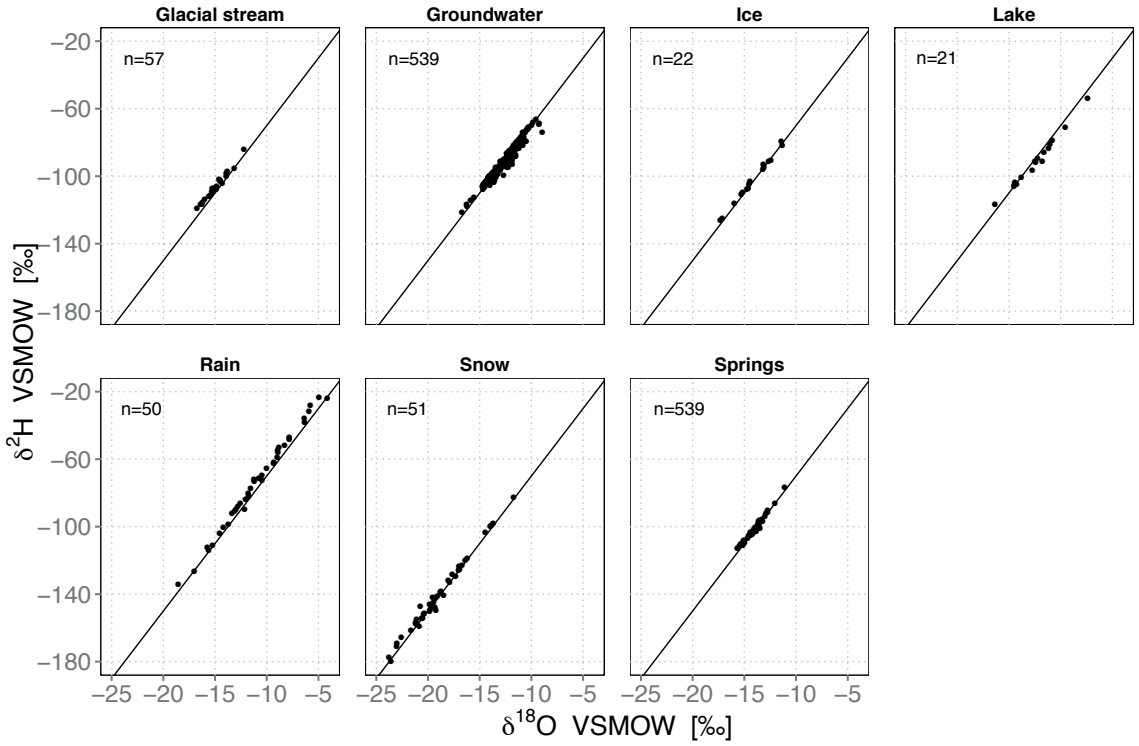

Figure 5.13: Relation between deuterium (δ^2H) and oxygen-18 (δ^{18}O) of different water types at the test site (2013 - 2014).

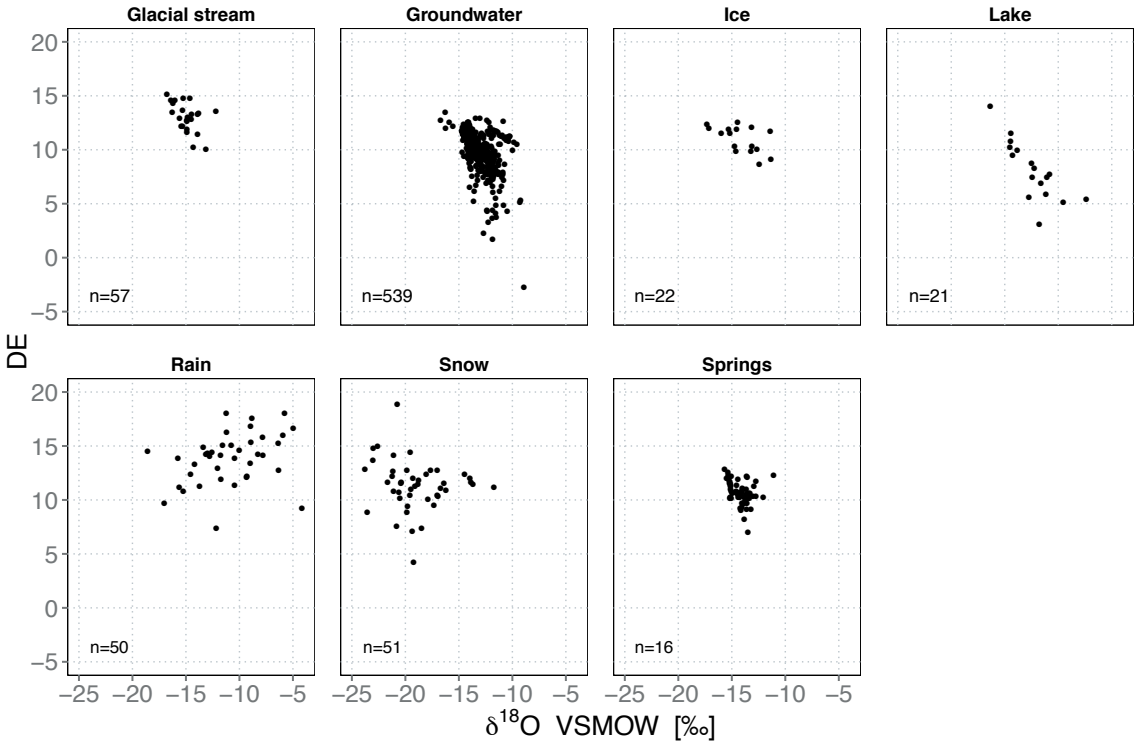

Figure 5.14: Relation between DE and δ^{18}O of different water types at the test site (2013 - 2014).

It is apparent that the majority of samples lie above the GMWL (Fig. 5.13). Especially summer and winter precipitation lie almost always over GMWL. In contrast, samples from groundwater and lakes lie commoner below GMWL, indicating evaporation processes. Summer & winter precipitation build the entire range of ^{18}O. These samples also have the highest DE values aside from few glacial stream samples (Fig. 5.14).

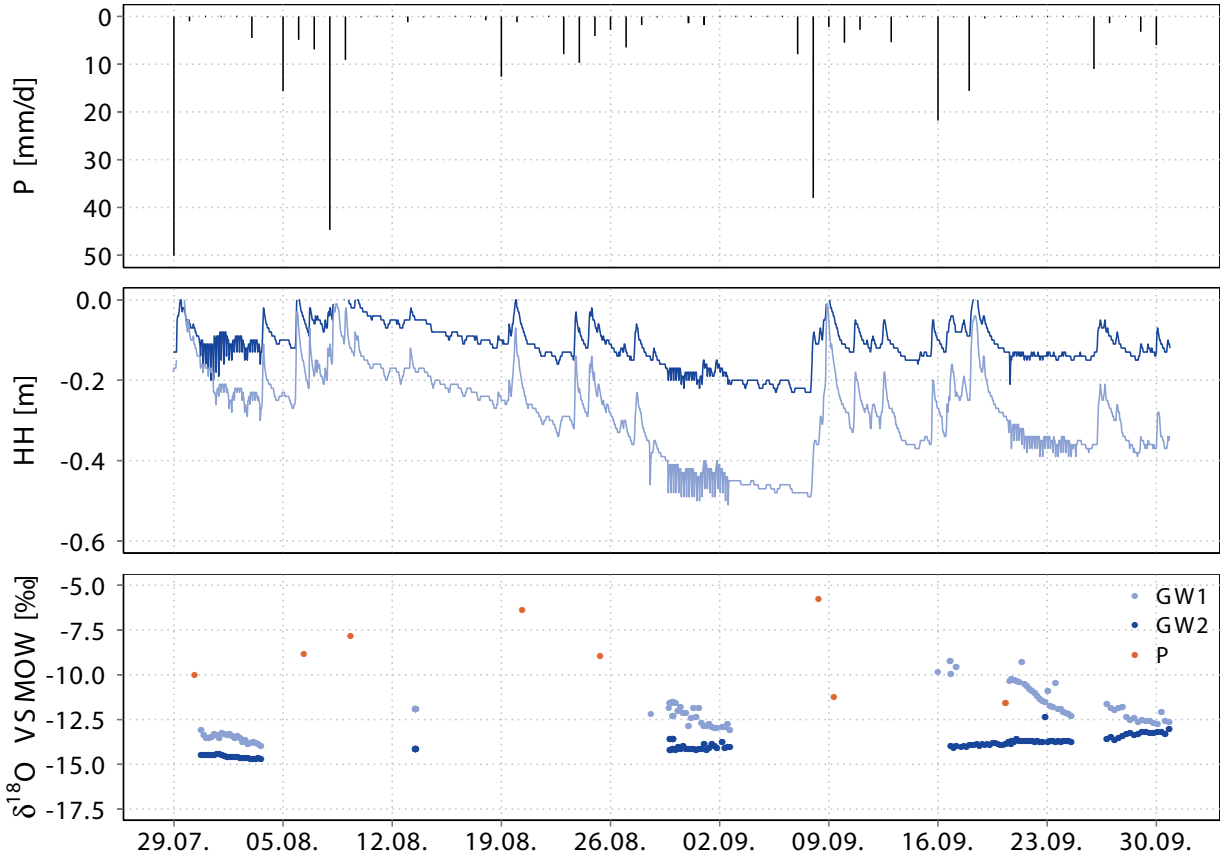

Figure 5.15: Evolution of oxygen-18 (^{18}O) during sampling campaigns 2013 for monitoring wells GW1 & GW2, as well as the ^{18}O input signal from precipitation (P samples were taken at the Albert-Heim hut mostly every day at 8 : 00 am when P $>$ 10 mm); sampling campaigns can be seen clearly at the variations in HH. The sampling campaign from 16.09.2013 till 20.09.2013 gave only three samples for GW1. GW1 is 1.5 m fully filtered (GL = 2365.7 m a.s.l.) & GW2 partly filtered from 1 to 2 m depth (GL = 2365.05 m a.s.l.), see Fig. 4.1.

Fig. 5.15 and 5.16 show the evolution of ^{18}O during sample campaigns for monitoring wells GW1 and GW2 as well as the time series of HH. Daily precipitation is illustrated in the same figure as input/recharge variable triggering hydrochemical dynamics. ^{18}O values for precipitation samples are also shown. Here, only the daily precipitation samples from Albert-Heim hut are considered in order to see how the aquifer reacts on the incoming isotope signal. The altitude difference between the test site and the hut is about 200 m. This should be taken into account when comparing the isotope signals. The altitude effect for ^{18}O can be assumed to 0.2 ‰/100 m (Schürch et al. 2003). Various sampling times with the automated water sampler go hand-in-hand with small decreases in HH. This effect is strongest at monitoring well GW1.

On average, every single sampling time, HH decreases of 0.1 m in GW1, whereas the variations in GW2 are only a few centimeters. GW1 shows a higher response to precipitation events in its HH, because HH at GW2 is closer to its GL due to the different absolute heights of the wells (GW1: GL = 2365.7 m a.s.l.; GW2: GL = 2365.05 m a.s.l.; see Fig. 4.1).

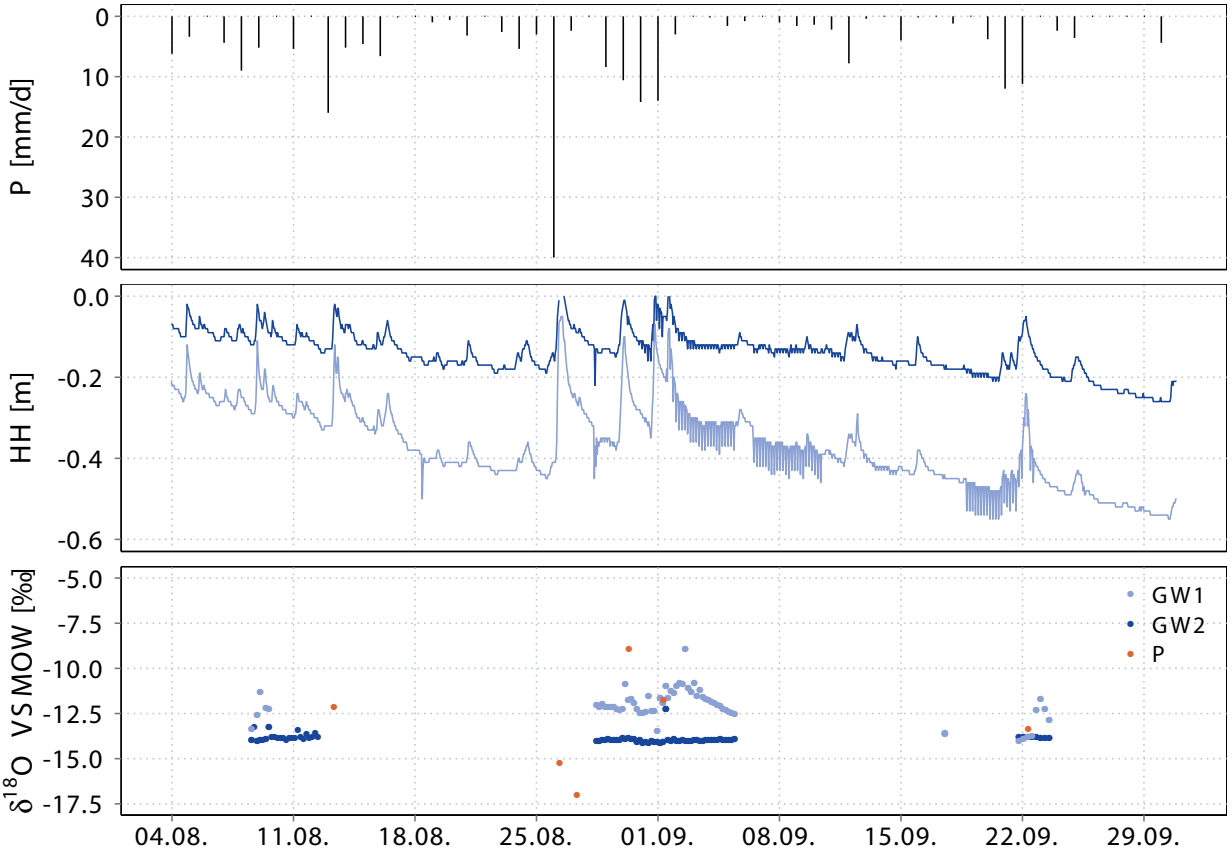

Figure 5.16: Evolution of oxygen-18 (^{18}O) during sampling campaigns 2014 for monitoring wells GW1 & GW2, as well as the ^{18}O input signal from precipitation (P samples were taken at the Albert-Heim hut every day at 8 : 00 am when P $>$ 10 mm); sampling campaigns can be seen clearly at the variations in HH. Samples have not been taken at each sampling campaign. GW1 is 1.5 m fully filtered (GL = 2365.7 m a.s.l.) & GW2 partly filtered from 1 to 2 m depth (GL = 2365.05 m a.s.l.), see Fig. 4.1.

GW1 shows a clear depletion in ^{18}O during decrease of HH, after peaks caused by precipitation events. GW2 shows, however, no such peak but mostly a moderate enrichment of ^{18}O. It seems that both wells are approaching each other in ^{18}O signal after precipitation events. When dividing the isotopic signal of the whole groundwater samples into GW1 and GW2 (see Fig. 5.17) a clear difference between these two monitoring wells is detectable. Whereas GW1 reflects the ^{18}O input signal from rain, δ^{18}O values from GW2 are closer to those of snow. Additionally, the range of δ^{18}O is wider for samples from GW1.

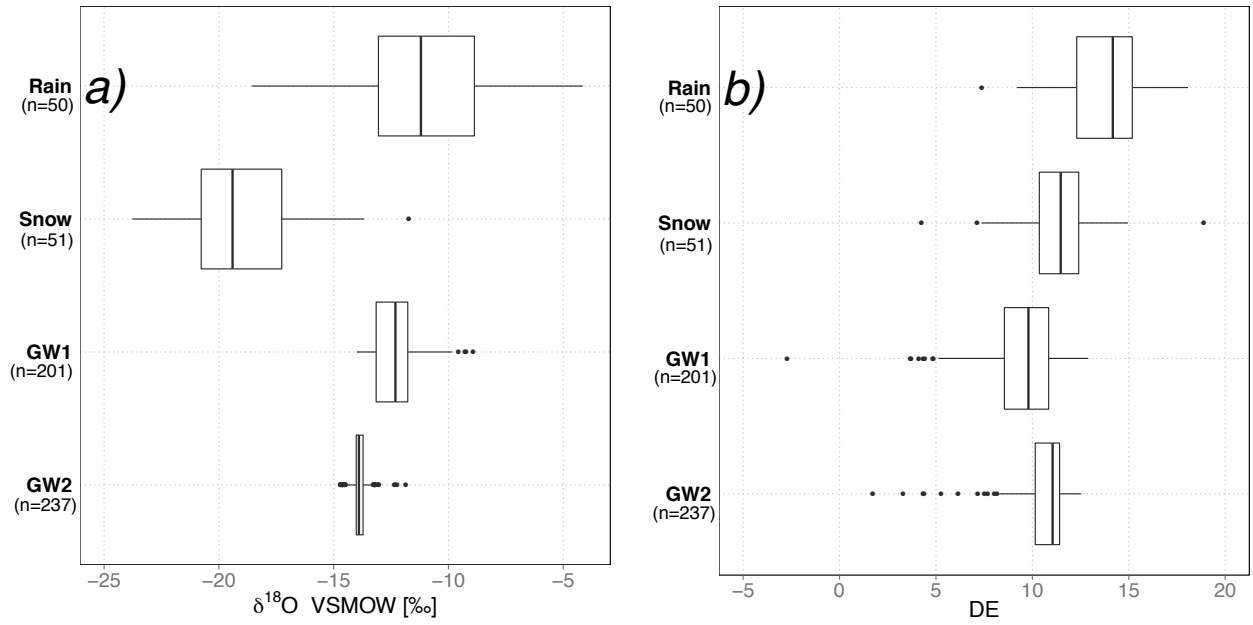

Figure 5.17: δ^{18}O and DE values for GW1 & GW2 compared to the input signals from rain and snow. The different isotopic composition at monitoring well GW1 & GW2 indicating different sources of recharge. Whereas GW1 reflects the ^{18}O input signal from rain, δ^{18}O values from GW2 are closer to those of snow (boxplot: median, box = 1st & 3rd quartiles, wiskers = 1.5 · interquartile range).

Tab. 5.2 presents mean δ^{18}O and mean DE values for the remaining monitoring wells. It documents, that the deeper wells (GW6 & GW7) show higher DE values. GW6 shows also depleted δ^{18}O values, than the direct adjacent wells GW1 & GW8. The same is visible for GW7 & GW9.

Table 5.2: Mean δ^{18}O and DE values for all monitoring wells, number of samples (n) as well as the filtering given as absolute heights [m a.s.l.].

monitoring well	**n**	**filtered zone [m a.s.l.]**	**δ^{18}O VSMOW**	**DE**
GW1	201	2365.70 - 2364.20	-12.31	10.4
GW2	237	2364.15 - 2363.15	-13.86	10.59
GW3	6	2356.33 - 2364.33	-14.24	10.02
GW6	3	2364.05 - 2363.05	-13.86	11.63
GW7	3	2363.84 - 2362.84	-14.76	12.09
GW8	3	2365.71 - 2364.71	-12.69	10.09
GW9	3	2365.58 - 2364.56	-12.68	10.27

5.5 Saturated hydraulic conductivity of the alluvial aquifer

Tab. 5.3 shows the results from the slug and infiltration tests with the Guelph-Permeameter. Slug tests were analyzed using the methods of Bouwer & Rice (1976) and Hvorslev (1951). The measurements with the Guelph-Permeameter were analyzed using a calculating sheet from (Soilmoisture Equipment Corp. 2012)). The values of K_{sat} from infiltration tests with the Guelph-Permeameter are throughout smaller ($3.3 \cdot 10^{-6}$ m/s - $4.8 \cdot 10^{-5}$ m/s) than those from slug tests ($1.3 \cdot 10^{-5}$ m/s - $1.8 \cdot 10^{-4}$ m/s). Both of these methods should not be compared too strictly, because the measurements with the permeameter were conducted in unsaturated zone - in our case the upper 10 - 30 cm - whereas slug tests are conducted in the monitoring well, which is filtered in the saturated zone. Despite these differences, all methods indicate highest K_{sat} for site B & C and smaller values for site A, which is near monitoring well GW1 (Fig. 4.4).

Table 5.3: Saturated hydraulic conductivity at three different places at our test site (see Fig. 4.4), measured with slug tests and infiltration tests with a Guelph-Permeameter. Slug test were analyzed using methods of Bouwer & Rice (1976) and Hvorslev (1951).

Site	**Slug tests**		**Guelph-Permeameter**
	Bouwer & Rice [m/s]	**Hvorslev** [m/s]	[m/s]
A	$1.3 \cdot 10^{-5}$	$2.2 \cdot 10^{-5}$	$3.3 \cdot 10^{-6}$
	$1.3 \cdot 10^{-5}$	$2.1 \cdot 10^{-5}$	
	$1.5 \cdot 10^{-5}$	$2.5 \cdot 10^{-5}$	
B	$1.2 \cdot 10^{-4}$	$7.2 \cdot 10^{-5}$	$3.3 \cdot 10^{-5}$
	$1.3 \cdot 10^{-4}$	$1.3 \cdot 10^{-4}$	
	$1.8 \cdot 10^{-4}$	$8.5 \cdot 10^{-5}$	
C	$1.8 \cdot 10^{-4}$	$1.1 \cdot 10^{-4}$	$4.8 \cdot 10^{-5}$
	$1.2 \cdot 10^{-4}$	$1 \cdot 10^{-4}$	

5.6 Extend and layering of the alluvial aquifer

The results from the ERT measurements 2012 (Fig. 5.18) indicate an aquifer extent of approximately 200 x 160 m and a depth of 20 m. In October 2014 further measurements were conducted. This time the spacing between the electrodes was 0.5 m. This smaller spacing results in a higher resolution of the upper areas. Fig. 5.19 shows a clear layer boundary at a depth of approximately 0.4 m and a further one at about 1 m depth. The sites of slug test A (GW1) and C are also marked.

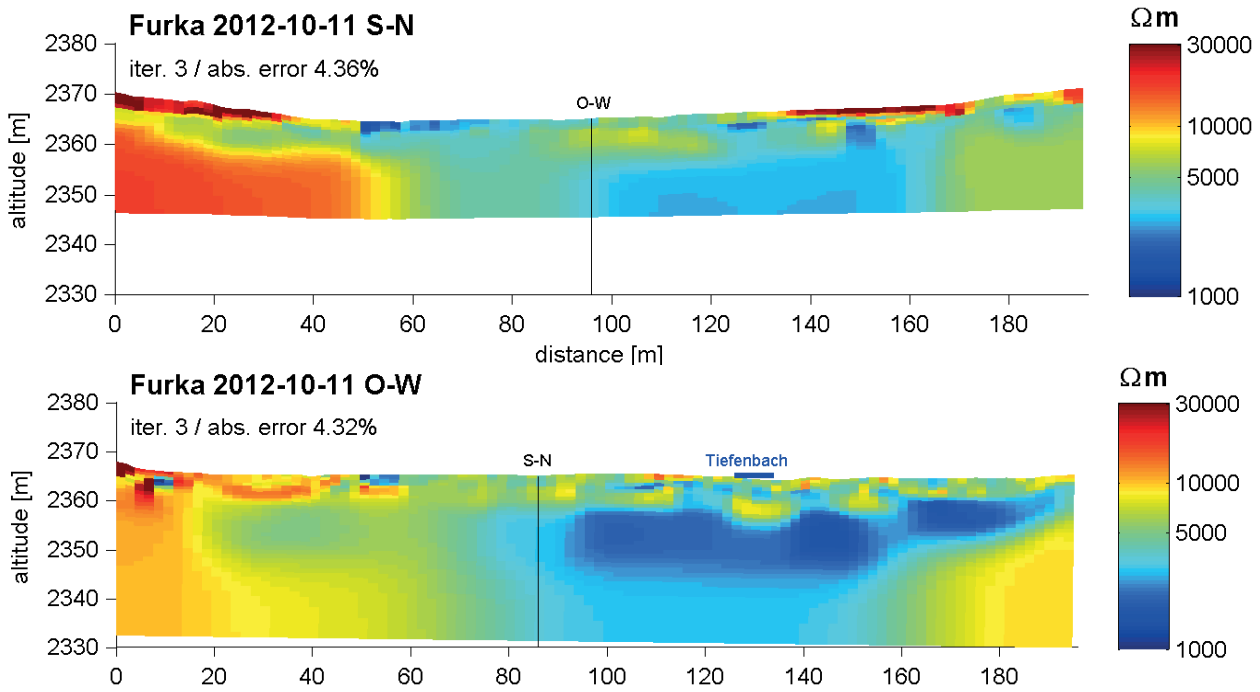

Figure 5.18: Results of geophysical survey (October 2012), using *electrical resistivity tomography* (ERT). Two transects (E-W & S-N) were applied with each 100 electrodes and a spacing of 2 m.

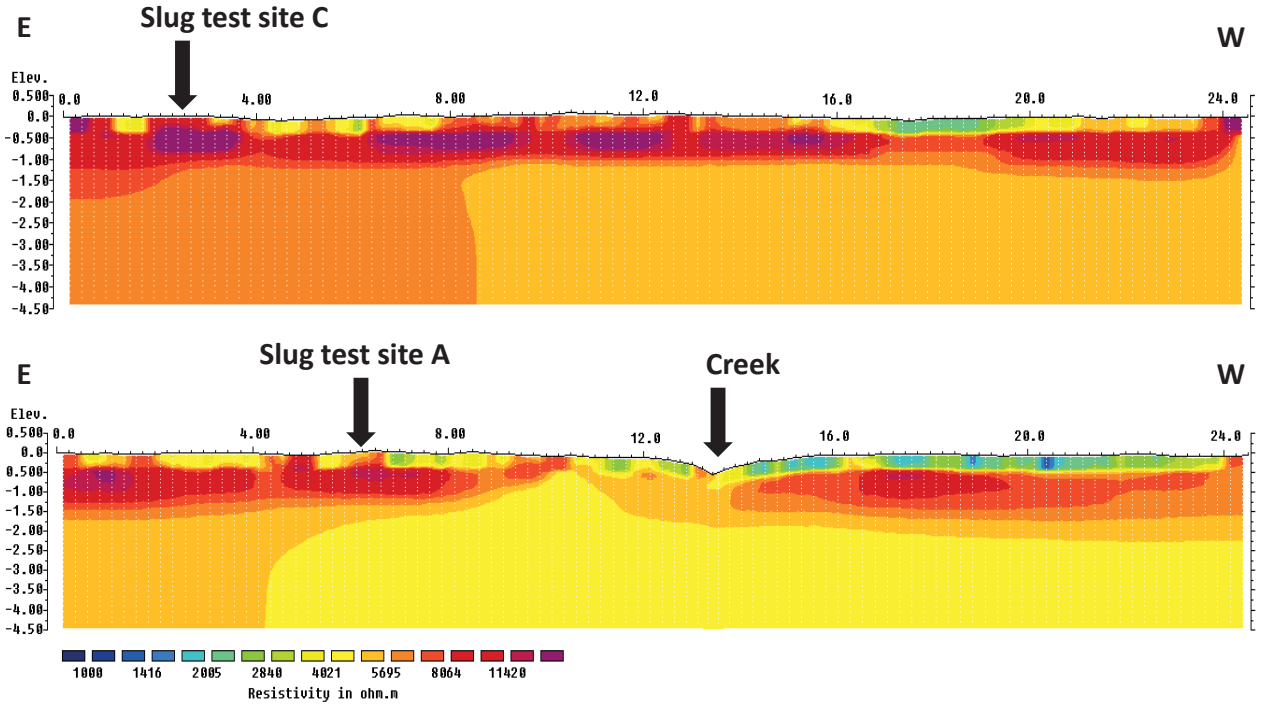

Figure 5.19: Results of geophysical survey (October 2014), using *electrical resistivity tomography* (ERT). Two similar aligned transects (E-W) were applied with 50 electrodes each, a spacing of 0.5 m and a overlap of 2 m.

5.7 Estimated storage capacity for the alluvial aquifer

The storage capacity of the alluvial aquifer can be estimated using equation 6 (p.21). The input variables are the total area of the aquifer ($32'000\,m^2$) and the mean depth (20 m), resulting from the ERT measurements 2012. The drainable porosity of the alluvial aquifer was estimated on 0.3. The total storage capacity of the aquifer is estimated to be in the order of 12.8 - 25.6 $\cdot$ $10^4\,m^3$. Because only a certain part of the aquifer could contribute to runoff of glacial stream, it was divided into an active and passive part. The active aquifer has a depth of approximately 3 m, calculated with mean ground level of 2365.4 m a.s.l. (average of the 9 monitoring wells) and 2362.44 m a.s.l. as gauge zero at the catchment outlet. This leads to a storage capacity of 1.92 - 3.84 $\cdot$ $10^4\,m^3$. The recharge volume by snowmelt 2014 was also calculated. During the snowmelt 2014, HH of GW2 increased from approximately -1 m to 0 m. This change in saturated thickness leads to a recharge volume of 0.64 - 1.28 $\cdot$ $10^4\,m^3$.

Table 5.4: Estimation of water storage volume (V_S) of alluvial aquifer divided in total, active & passive part as well as recharge volume of snowmelt 2014. Calculation from total area (A), drainable porosity (n) and thickness (d).

Unit	**A [10^4 m^2]**	**n**	**d [m]**	**V_S [10^4 m^3]**
total aquifer	3.2	0.3	20	12.8-25.6
active part	3.2	0.3	3	1.92-3.84
passive part	3.2	0.3	17	10.88-21.76
recharge by snowmelt 2014	3.2	0.3	1	0.64-1.28

6 Discussion

6.1 Characteristics of the alluvial aquifer

Values for saturated hydraulic conductivity (K_{sat}) of the periglacial floodplain measured with slug tests ranged from $1.3 \cdot 10^{-5}$ m/s near monitoring well GW1 to $1.8 \cdot 10^{-4}$ m/s near the glacial stream. These values are similar to those measured from Magnusson et al. (2012) for a glacier forefield of the adjacent Dammagletscher and Clow et al. (2003) for an alpine aquifer in Loch Vale, Rocky Mountains. Furthermore, Cooper et al. (2002) found similar values for K_{sat} in moraine and fluvio-glacial sediments in a floodplain in front of the glacier Finsterwalderbreen, Svalbard. Averaged K_{sat} are roughly similar for site B ($1.4 \cdot 10^{-4}$ m/s (Bower & Rice), $9.7 \cdot 10^{-5}$ m/s (Hvorslev)) & site C ($1.5 \cdot 10^{-4}$ m/s (Bower & Rice), $1.1 \cdot 10^{-4}$ m/s (Hvorslev)). These sites show also higher values than site A ($1.4 \cdot 10^{-5}$ m/s (Bower & Rice), $2.3 \cdot 10^{-5}$ m/s (Hvorslev)), which is in the vicinity of monitoring well GW1. For site B the highest values were expected. This site is most influenced by glacial stream cause of the deeper ground level (GL) (about 0.6 m deeper than site A; see Fig. 4.1, p.12). Hence, it is often flooded when runoff from glacial stream increases and the stream will deposit a lot of sediments there. This sedimentation area could be seen well on the orthophoto (Fig. 4.4, p.17). K_{sat} measured with infiltration test by Guelph-Permeameter are throughout smaller than those measured with slug-tests. Both of these methods should not be compared too strictly, because the measurements with Permeameter are conducted in unsaturated zone, in our case the upper 10 - 30 cm, whereas slug tests were conducted in the monitoring well, which was filtered in the saturated zone.

6.2 Seasonal storage dynamics

Based on the time series from Fig. 5.1 (p.24) conclusions can be drawn about the storage dynamics of this alluvial aquifer. The course of the year can be divided into three different parts: (1) summer, (2) winter & (3) snowmelt. These phases are highlighted in the following figure (Fig. 6.1). First one is the part of summer time without snow cover (white). It is characterized by fluctuations in HH coincident with different precipitation events. This causes also fluctuations in EC. The start of the summer period can be explicit detected by rising T_{GW}. During snow covered time T_{GW} is about 0 °C. Remarkable is T_{GW} of about 10 °C in a height of 2365 m a.s.l. Similar T_{GW} for alpine groundwater can also be found in (Clow et al. 2003, Ward et al. 1999). Generally, T_{GW} approximately reflects the mean annual air temperature (MAAT) at the area. The MAAT for a comparable station (Gütsch ob Andermatt, 2283 m a.s.l.) for the norm period 1981 - 2010 is 0.4 °C (MeteoSwiss 2015). One reason for such high T_{GW} is, that the soils are relatively thin. Furthermore there are no plants or trees which provide shade resulting in direct radiation input. After snowmelt there is a lot of rotten gras on the alluvial plain. Its dark color, combined with long days and strong radiation input during this times could also support such abrupt increase in T_{GW}.

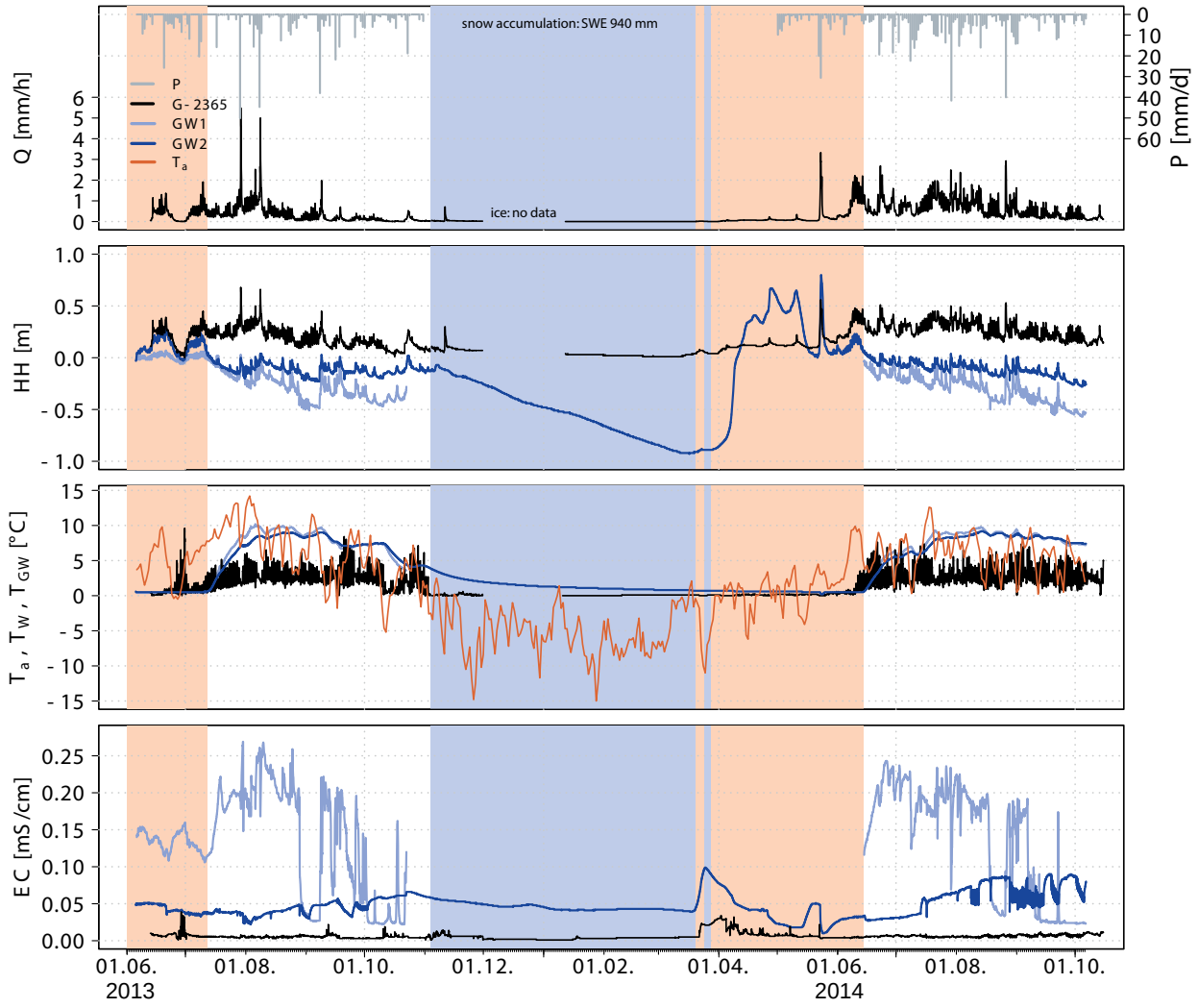

Figure 6.1: Mean daily precipitation (P) & mean daily air temperature (T_a), runoff from glacial stream [mm/d], hydraulic head (HH, depth to groundwater), groundwater temperature (T_{GW}) and electrical conductivity (EC) at monitoring well GW1 & GW2 as well as hydraulic head (water level above gauge zero), water temperature (T_W) and electrical conductivity (EC) from glacial stream; HH, T_{GW} and EC measured in 15 min time steps at monitoring wells GW1 & GW2; GW1 is 1.5 m fully filtered (GL = 2365.7 m a.s.l.) & GW2 partly filtered from 1 to 2 m depth (GL = 2365.05 m a.s.l.) see Fig. 4.1; HH, T_W and EC measured in 5 min time steps at glacial stream; data from glacial stream and monitoring wells are aggregated to hourly values; runoff is calculated by p/q - ratio, validated for medium and high flows with salt and uranin dilution; not validated for low flows. Time series is divided in three different storage phases (summer = white, winter = blue & snow melt = orange).

With the first snow fall around October to November, the aquifer system changes to the winter part, respectively the time of continuous snow cover (blue). This period is characterized by continuously falling groundwater temperatures to almost 0 °C, constant EC values and a continuously falling HH. This part is interrupted by a EC peak on 24.03.2014 accompanied with a moderate rise in HH. The same signal is also visible at the glacial stream. According to the weekly report from SLF, the weather in this period was mild and the snow cover on eastern slopes < 2700 m was 0 °C-isothermal (SLF 2014). This could lead to local snowmelt on the adjacent slopes. The resulting melt water could pushes the groundwater into the aquifer.

Another possible explanation for this EC-peak could be a rain on snow (ROS) event, which results in a leaching of ions from the snow cover due to the percolating rain water. A few days before, the mean daily air temperature rised temporarily from negative values up to 2.1 °C. Thus, it was possible to have liquid precipitation. Kristiansen et al. (2013) found similar rises in EC during times of snow cover for groundwater in front of a glacier in southeast Greenland caused by a ROS event. They also noticed a lag of few days between the ROS event and the EC-peak.

Normally, the aquifer is seasonally decoupled from its recharge, caused by the continuously accumulation of snow throughout the winter season. This changes with the ripening of the snow pack and the aquifer gets strongly recharged at the peak snowmelt. The period of snowmelt (orange) can be clearly identified by the rapidly rise in HH even above the ground surface. Because the soil is not frozen, the meltwater infiltrates into the aquifer. Measured T_{GW} at the beginning of the continuously snow accumulation (15.10.2013) in the winter season 2014 lie over 6 °C (see Fig. 5.8, p.31). Thus, freezing of the soil is prevented by early snowfall and the resulting isolation of the snow cover. Bayard et al. (2005) found, that the late autumn and early winter meteorological conditions are decisive for the development or absence of soil frost. If the soil frost remains until the end of winter, it may reduces the groundwater recharge by up to 25 %. The fact that the aquifer becomes completely filled during the snowmelt and that it shows a decrease in HH over the summer period would suggest, that the groundwater recharge is dominated by the snowmelt. The outflow behavior of the aquifer during wintertime is nearly linear. That indicates either a lost of groundwater through fractures in bedrock or an decreasing porosity with depth. A potential percolation of groundwater into the fractured bedrock could not be clarified through this study. Therefore, it would be useful, for example, to have monitoring wells filtered in the passive part of the aquifer. However, Ofterdinger et al. (2004) used environmental tracers, such as stable isotopes of water to identify groundwater recharge to fractured granite in an adjacent catchment. They sampled groundwater in the Bedretto Tunnel, which goes through the granite body of the western Gotthard Massif. They found that accumulated winter precipitation and glacial meltwater may contribute significantly to recharge of deep groundwater.

A second option for the linear outflow behavior is presented in Fig. 6.2. (a) illustrates the outflow with constant porosity. Due to the decreasing pressure of the water column, the outflowing volume per time decreases. This leads to a non-linear outflow. (b) shows a linear outflow due to decreasing porosity with depth. This implies, similar to (a), a decreasing water volume lost per time. However, the HH decreases constantly because the water volume per depth unit also decreases. This case is comparable with a funnel.

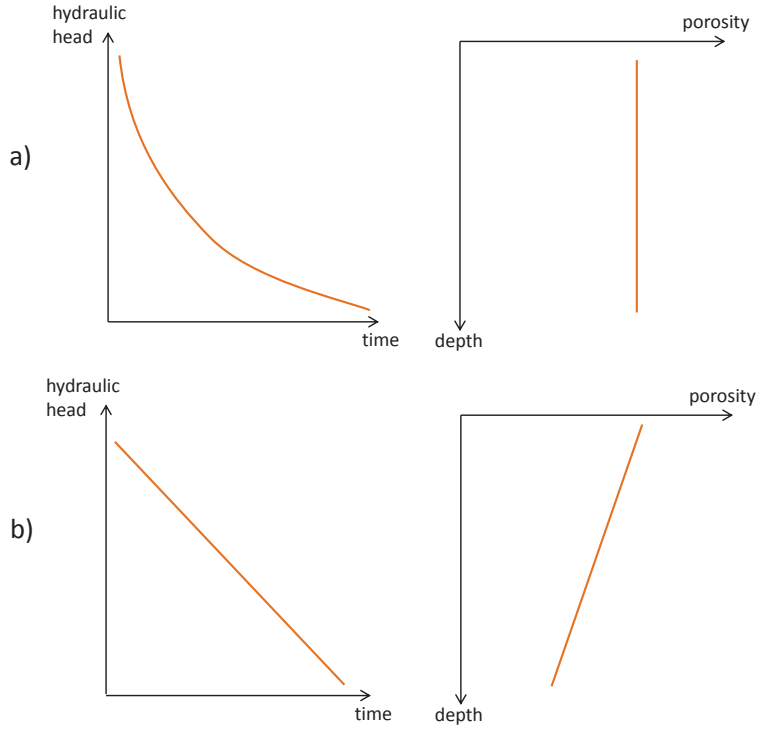

Figure 6.2: Schematic representation of the effect of decreasing porosity with depth on outflow behavior of the alluvial aquifer during winter time. The first case with constant porosity (a) assumes, that percolation of groundwater through fractured rock is negligible. Its nonlinear decreasing in HH is due to the decreasing pressure head with time. Linear decreasing of HH (b) could be due to decreasing porosity with depth, which leads to decreasing volume lost per time or due to a higher proportion of percolating groundwater through fractured bedrock.

Fig. 6.3 provides a schematic overview of the dominant reservoirs, processes and regulators for the studied alpine alluvial aquifer. The snow cover presents a large reservoir of water. The early snowfalls even prevent soil freezing, due to the isolation effect of the snow cover. A frozen soil would reduce the infiltration of melt water (Bayard et al. 2005). Thus, the snow cover can be regarded as an regulator. The recharge of the alluvial aquifer is dominated by snowmelt. During the snowmelt the aquifer becomes completely filled. If the infiltration capacity is reached, the groundwater could even exfiltrates into the snowpack. Due to the level differences, the aquifer should be divided in an active and an passive part. Only groundwater from the active part can contribute to the runoff off the glacial stream by exfiltration. According to the hydraulic head, stream water could also infiltrate.

The adjacent hillslopes have also an impact on the alluvial aquifer in terms of providing base flow and saturated overland flow. Depending on fracture frequency & -orientation of the bedrock, groundwater may get lost through percolation.

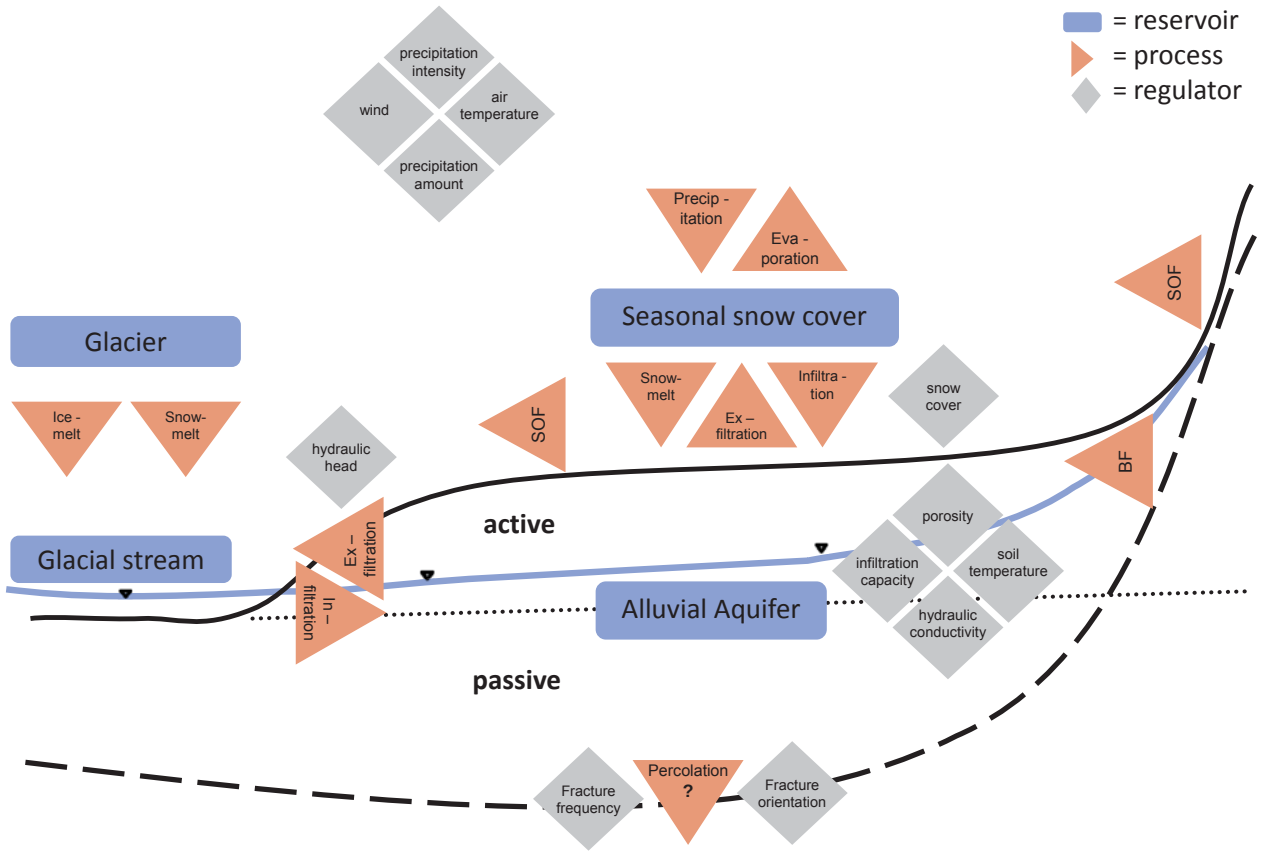

Figure 6.3: Schematic overview of reservoirs, processes & regulators for the studied alpine alluvial aquifer. Between the reservoirs (blue rectangles) there are directed processes (orange arrow in direction) which are regulated by regulators (grey diamonds). Additionally, the boundary between the active and the passive aquifer (dotted line) as well as the boundary to the underlying bedrock (dashed line) are plotted. SOF = saturated overland flow, BF = base flow.

Isotopic composition

^{18}O values of precipitation show large seasonal variations of $\sim 20\,‰$ with values ranging from $\sim -4\,‰$ during summer down to $\sim -24\,‰$ during winter months (see Fig. 5.11, p.34). These findings are in accordance with the results from Mueller et al. (2013), who measured similar ^{18}O values of summer and winter precipitation in 4 micro-catchments in adjacent Urseren valley for the season 2010/2011. Most of our precipitation samples (snow and rain) show DE values in the range of 10 to 15 (see Fig. 5.12 on p.35). This is consistent with the results from Flaim et al. (2013). They found, that DE shown a clear altitude effect ($\sim 0.32/100\,m$). Consequently, precipitation in same height as our test site (2365 m a.s.l.) should show DE values in range of $\sim 12 \pm 2$. The isotopic composition of precipitation corresponds also well with findings from Schürch et al. (2003).

They studied precipitation samples along an elevation gradient from the station Meiringen (632 m a.s.l.) over Gutannen (1055 m a.s.l.) to Grimsel (1950 m a.s.l.). These station are situated in the near of our test site and therefore well suited for comparison. ^{18}O values for ice and glacial stream samples are well matched, as the main source of the glacial stream is the ice melt. The groundwater samples show different values. Those from monitoring well GW1 indicate summer precipitation as the main recharge source, whereas the samples from GW2 are closer to the signal from snow. This is consistent with the water level fluctuations. The soil at GW2 is saturated mostly the whole summer. In contrast, the ground level of monitoring well GW1 is about 60 cm higher than GW2 resulting in the evolution of an unsaturated zone. Thus, rain water could infiltrate, whereas the soil of monitoring well GW2 is almost already saturated. Furthermore, the mean $\delta^{18}O$ and DE values, presented in Tab. 5.2, indicate two different flow systems in the aquifer. (1) The shallow one is mainly recharged by summer precipitation, whereas the recharge from the deeper one (2) is dominated by snowmelt. The variability from the $\delta^{18}O$ and DE values for GW1 (shallow flow system) is larger than those for GW2 (deep flow system). This is plausible, since the shallow flow system is more influenced by several precipitation events, whereas the deeper one is mainly influence by a single snowmelt. Contrary to the mainly saturated conditions at GW2, the DE values indicates less evaporation influence than at GW1 which could be affected by the permanent supply of water due to the less absolute height. The median of DE for GW2 is very close to that of snow and both indicating less evaporation, since typically DE values for this height are $\sim 12 \pm 2$ (Flaim et al. 2013). Unfortunately, there was no sampling campaign during the snowmelt. Such samples may highlight a significant shift in the isotopic signature during the snowmelt.

6.3 Hydrochemistry

The hydrochemical composition of the groundwater has a highly spatial and temporal variability. While monitoring well GW1 shows high fluctuations in EC from 0.025 to 0.275 mS/cm, the other monitoring wells GW2 & GW3 show relative moderate values <0.1 mS/cm. The hydrochemistry at GW1 may be affected by GW level fluctuations (see Fig. 5.4, p.27). The variations in EC occurs only at GW levels higher -0.35 m. The increases in HH above this level are mainly affected by summer precipitation. Monitoring well GW1 has the highest GL and it is also filtered in the upper section. Thus, there is a unsaturated zone almost the whole summer. However, since precipitation shows not such high values of ions, it can be assumed that the soils from the distinctive unsaturated zone leaches ions into the groundwater. Especially calcium (Ca^{2+}) seems to be responsible for the fluctuations in EC (see Fig. 5.5, p.28). The soils at this floodplain are relative young. After the little ice age (LIA) in 1850, the Tiefengletscher started retreating and the depression could be filled with alluvial sediments. These young soil could leach a high amount of Ca^{2+}. To clarify if the upper soil near GW1 is enriched of Ca^{2+}, a soil sample was taken.

The results from IC for the soil sample are not gratifying (see Tab. 5.1, p.29). The first two preparations show enriched values for K^+ and Cl^-, due to contamination with KCL from the pH measuring device, since KCl is the stock solution for the pH probe. It is striking, that Ca^{2+} shows lower values for the lower dilution. The most ions show more or less the same concentration no matter which dilution. A reason for this could be, that the soil was not sifted prior the preparation. Thus, the different preparations could have different amounts of fine earth. The glacial stream shows very low values of EC (Fig. 5.4, p.27). This was expected because the runoff is mainly composed by glacier- and snowmelt. Obvious variations in EC occur only at low HH (0 to 0.1 m). This can be attributed to the fact, that the groundwater contribution to runoff is higher during low flows, which is usually the case during the winter. The increased contribution from groundwater to base flow could also be seen at silica concentrations as well as in the isotopic signal. Glacial stream has, aside from winter and summer precipitation, the lowest concentrations of silica from the samples. This is because its runoff during the summertime (mainly sampling period) is primarily provided by glacier and snow melt. Those values from glacial stream, which are higher than ~ 0.1 mg/L are samples during wintertime. This indicates higher groundwater contribution to runoff caused by the negligible glacier and snow melt in winter. Groundwater contribution could also be detected at the creeks. These samples show higher concentration than the springs, where they originate from. In contrast to the other water types, groundwater shows the highest silica values as well as the highest range. These high values result from the longer contact times with the soil than the other water types. There are, however, groundwater samples with relative low silica concentrations. The samples, which are the lower outliers are taken during a sampling campaign at the end of August 2014 where it was snowing during the night and melting next day. The samples equally shows significant higher DE values indicating a different source of water.

6.4 Relevance of alluvial aquifers for alpine watershed

Glaciers are important for providing base flow during the summer period. With ongoing glacier retreat, their contribution to the base flow get reduced. The question is, if such alluvial aquifers may partially compensate the reduction of the base flow through retreating glaciers. Clow et al. (2003) determined a contribution of talus to streamflow during low flow of about 75 % using tracer test and discharge measurements. Hood & Hayashi (2015) estimated storage volumes for moraines, talus and meadow of an entire catchment within the Lake O'Hara watershed, Canada. The estimated peak storage amount (60 - 100 mm) was relative small compared to the pre-melt snow water equivalent but significant compared to the winter baseflow (< 0.5 mm/d), indicating the importance of these groundwater storages for low flows. The alluvial aquifer which was investigated in this study has an extension of approximately $32'000\,m^2$, that is approximately 0.5 % of the entire catchment.

The spatial contribution of such aquifers to the total catchment area is estimated of about 10 % based on the slope (see. Fig. 3.4, p.8). Unfortunately, we have no calibrated p/q-ratio for low flows. Field observations, however, indicate a low flow during winter of approximately 100 l/s respectively 1.37 mm/d. To provide such an base flow for the winter time (approximately 6 month) at the Tiefenbach catchment (6.3 km^2), alluvial aquifers with an percentage share of 10 % of the total catchment should have an saturated active part of about 8 m (see Tab. 6.1). The active part of the studied aquifer is only about 3 m but we estimate for reservoirs closer to the Tiefengletscher bigger active parts. There are for example large moraine fields with > 30 m thickness and springs with discharges > 100 l/s. Discharge measurements on these springs would be very useful to quantify their storage capacity.

Table 6.1: Estimated groundwater level decrease for providing low flow in different time scales. The low flow is estimated at 100 l/s respectively 1.37 mm/d. Q_{Unit} is calculated with ratio between catchment area (6.3 km^2) and unit multiplies with low flow (1.37 mm/d); the resulting HH decrease of each unit is calculated by Q_{Unit} / porosity (0.3).

percentage share of catchment	**area [m^2]**	**Q_{Unit} [mm/d]**	**HH decrease**				
			per day [mm]	**1 month [mm]**	**2 months [mm]**	**4 months [mm]**	**6 months [mm]**
~ 0.5	32'000	270	900	27000	54000	108000	162000
1	63'000	137	457	13700	27400	54800	82200
5	315'000	27	90	2700	5400	10800	16200
10	630'000	14	47	1400	2800	5600	8400
20	1'260'000	7	23	700	1400	2800	4200

Recent studies e.g. Clow et al. (2003), Hood & Hayashi (2015) show, that the retreat of the glaciers induce new groundwater reservoirs such as talus, moraines & alluvial aquifers. They all provide a non-negligible amount of groundwater. Fig. 6.4 provides an schematic graph of these storages as well as their corresponding time scales. Since there are not enough measurements to the respective residence times, the time scales should be regarded as estimation. Glaciers are a typical long term storage, whereas the seasonal snow cover represents an intermediate-term storage, ranging from days to year. If glaciers retreat, new lakes or alluvial aquifers can be formed in bed depressions. The alluvial aquifer can be regarded as an intermediate-term storage, even if groundwater in the passive part of the aquifer can have longer residence times depending on the magnitude of percolation through fractured bedrock. Mean residence times for deep groundwater were estimated from (Ofterdinger et al. 2004) in order of 1 - 1.5 years. But they also detect rapid recharge from glaciated areas through fault zones.

McClymont et al. (2010) found relative short residence times of groundwater in meadow-talus complex, since the recharge volume from snowmelt and rainfall is several times higher than the total storage volume.

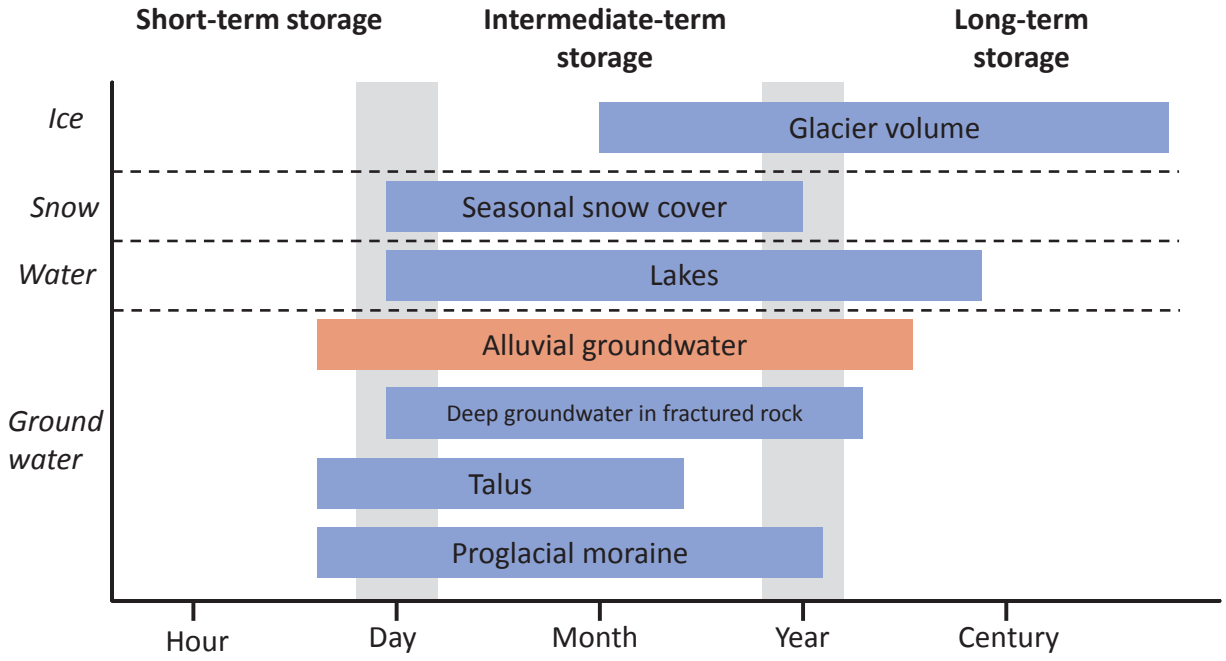

Figure 6.4: Schematic graph showing different water storages in alpine region and their corresponding time scales.

7 Conclusion

7.1 Findings

The study shows, that the groundwater recharge of the alluvial aquifer is mainly dominated by the snowmelt. During the snowmelt, the aquifer get completely filled and the groundwater even exfiltrates into the snowpack. The groundwater levels are very variable during the short summer period due to different precipitation events. Especially monitoring well GW1 reacts strongly on precipitation events, because there is a extended unsaturated zone. It is conceivable that such unsaturated zones may have a large buffering capacity for intense rainfalls. There are, however, sites with lower ground levels, such as GW2, which are almost the whole summer period saturated. Another difference between GW1 and GW2 is the hydrochemistry. GW1 shows large variations in the electrical conductivity (EC) whereas the variations at GW2 are relative moderate. The results from ion chromatography indicate, that EC is mainly affected by leaching of ions from the unsaturated soil. Especially Ca^{2+} shows a high correlation with EC, as it is representative for such young soils. Relative high groundwater temperatures (T_{GW}) of about 10 °C could be detected, which is a result of thin soils and direct radiation input through missing vegetation. That means, that the assumption that the T_{GW} reflects approximately (± 1 °C) the mean annual air temperature doesn't apply. These high T_{GW} may also accelerate the weathering rates. Such aquifers may provide low flows during winter or summer droughts, since they can store huge amounts of water. It depends on the thickness of the active part of the aquifer and the quantity respectively size of the aquifer. Here, only one alluvial aquifer was investigated. But additional groundwater level measurements on adjacent Lochbergbach & Wittenwasserenreus within this project suggest similar storage dynamics. In these two catchments also large flat sedimentation areas can be found, which is typical for formerly glaciated areas. Considering the world wide glacier retreat, it will be an important aim to investigate alternative water storages such as alluvial aquifers.

7.2 Reflection

This work can provide useful information for future field campaigns. The results from hydrochemistry show, that such an aquifer is highly heterogene. It depends on where monitoring wells are installed and if the filtering reaches into the saturated or unsaturated zone. It has been found practicable to create an image of the water level prior to the installation of the monitoring wells for example with the help of mini-piezometers. They are much easier to install and can be quickly removed. During the installation of the mini-piezometers with a hammer, hard layers could maybe detected. In this study, the assumption of a layer shift in about −0.4 m could be confirmed by conducting electrical resistance tomography (ERT). The ERT is a useful tool to estimate the extension and depth as well as different layers in the aquifer. To estimate the amount of groundwater contribution to the glacial stream, it would be useful to install gauge stations upstream and downstream the aquifer.

For investigating possibly percolation of groundwater into fractured bedrock, deeper monitoring wells which are filtered in the passive part of the aquifer are required. Thus, it would be possible to estimate residence times for example. Unfortunately, the conducted pumping tests were not successful. The distance of 2 m between the pumping and the observations wells was to large to see a distinctive difference in the hydraulic head (HH) on the observation well. Furthermore, pumping tests need a lot of time and materials which makes it challenging to conduct in alpine terrain. Slug test are therefore easier to conduct in such environments. It is possible to make several slug test a day, which would be more representative in such heterogeneous aquifers. The results show, that the period around the snowmelt affects the largest variations in HH, T_{GW} and EC. Thus, it would be interesting to conduct sampling campaigns prior, during and after the snowmelt. The large variations in EC at GW1 are mainly affected by Ca^{2+}. A distinctively rise in EC was detectable, when the water level rises above -0.4 m. The result of the ion chromatography of a soil sample was not gratifying. Three different preparations show significant differences which was probably due to the fact, that the soil was not sifted prior the preparation. For the future, it would be better to take samples below and above a layering. The best time for taking soil samples is probably the late autumn, when the water level is lowest. The CTD-online sensors proved to be very helpful. Having the actual data, it is possible to react quickly on events. Thus, it is possible to conduct specific sampling campaigns at times of high EC, T_{GW} or HH. Another great advantage is, that it is immediately visible if a sensor fails. With such sensors, it is also possible to equip several test sites without having to check or read out all sensors frequently. Additionally, the installation of time-lapse camera is very useful. With the camera it is possible to record the snow accumulation and the photos can provide useful information to interpret the data, for example fresh snow or flooding by the glacial stream. As the access to the alpine terrains is mostly difficult it is not easy to equip a huge number of aquifers. The study shows, that the measurements on a single monitoring well (GW2) during the whole course of the year can provide a lot of information about the storage dynamics. Thus, it might be useful to focus on selected aquifers with more detailed measurements and additionally equip a higher number of aquifers with just one sensored monitoring well.

References

Barnett, T. P., Adam, J. C. & Lettenmaier, D. P. (2005), 'Potential impacts of a warming climate on water availability in snow-dominated regions.', *Nature* **438**, 303–309.

Bayard, D., Stähli, M., Parriaux, A. & Flühler, H. (2005), 'The influence of seasonally frozen soil on the snowmelt runoff at two Alpine sites in southern Switzerland', *Journal of Hydrology* **309**(1-4), 66–84.

Bouwer, H. & Rice, R. (1976), 'A slug test for determining hydraulic conductivity of unconfined aquifers with completely or partially penetrating wells', *Water Resources Research* .

Clow, D., Schrott, L., Webb, R., Campbell, D. H., Torizzo, A. & Dornblaser, M. (2003), 'Ground water occurrence and contributions to stream ow in an alpine catchment, Colorado Front Range', *Ground Water* **41**(7), 937–950.

Cooper, R., Wadham, J., Tranter, M., Hodgkins, R. & Peters, N. E. (2002), 'Groundwater hydrochemistry in the active layer of the proglacial zone, Finsterwalderbreen, Svalbard', *Journal of Hydrology* **269**(3-4), 208–223.

Craig, H. (1961), 'Isotopic variations in meteoric waters', *Science* **133**(3465), 1702–1703.

Dansgaard, W. (1964), 'Stable isotopes in precipitation', *Tellus* **16**(4), 436–468.

DIN38405-D21 (1990), 'Photometrische Bestimmung von Kieselsäure (21) Deutsche Einheitsverfahren zur Wasser-, Abwasser- und Schlammuntersuchung DEV. Weinheim: Verlag Chemie.'.

Flaim, G., Camin, F., Tonon, A. & Obertegger, U. (2013), 'Stable isotopes of lakes and precipitation along an altitudinal gradient in the Eastern Alps', *Biogeochemistry* **116**(1-3), 187–198.

Froehlich, K., Gibson, J. J. & Aggarwal, P. (2002), Deuterium excess in precipitation and its climatological significance, *in* 'Study of Environmental Change Using Isotope Techniques. Proc. Intern. Conf', Citeseer, pp. 54–66.

Goldscheider, N. (2011), 'Alpine Hydrogeologie', *Grundwasser* **16**(1), 1–1.

Haeberli, W. & Beniston, M. (1998), 'Climate Change and Its Impacts on Glaciers and Permafrost in the Alps', *Ambio* **27**(4), 258–265.

Hood, J. L. & Hayashi, M. (2015), 'Characterization of snowmelt flux and groundwater storage in an alpine headwater basin', *Journal of Hydrology* **521**, 482–497.

Hosein, R., Arn, K., Steinmann, P., Adatte, T. & F{\"o}llmi, K. (2004), 'Carbonate and silicate weathering in two presently glaciated, crystalline catchments in the Swiss Alps', *Geochimica et Cosmochimica Acta* **68**(5), 1021–1033.

Hvorslev, M. J. (1951), 'Time lag and soil permeability in ground-water observations'.

Hydrological Atlas of Switzerland (2010), BAFU, Bundesamt für Umwelt, Map 2.2, Map 4.1 and 5.2.

Jansson, P., Hock, R. & Schneider, T. (2003), 'The concept of glacier storage: a review', *Journal of Hydrology* **282**(1-4), 116–129.

Jouzel, J. & Merlivat, L. (1984), 'Deuterium and oxygen 18 in precipitation: Modeling of the isotopic effects during snow formation.', *Journal of Geophysical Research. Atmospheres* **89**(D7), 11749–11757.

Kalbus, E., Reinstorf, F. & Schirmer, M. (2006), 'Measuring methods for groundwater - surface water interactions: a review', *Hydrology and Earth System Sciences* **10**(6), 873–887.

Kendall, C. & McDonnell, J. J. (1998), *Isotope tracers in catchment hydrology*, Elsevier, Amsterdam.

Kienzler, P. M. (2001), Experimentelle Untersuchungen zur chemischen Zusammensetzung oberflächennaher unterirdischer Abflusskomponenten im Bruggaeinzugsgebiet, Diploma thesis, Albert-Ludwigs Universität Freiburg i. Br.

Kristiansen, S. r. M., Yde, J. C., Bárcena, T. G., Jakobsen, B. H., Olsen, J. & Knudsen, N. T. (2013), 'Geochemistry of groundwater in front of a warm-based glacier in Southeast Greenland', *Geografiska Annaler: Series A, Physical Geography* **95**(2), 97–108.

Lauber, U., Kotyla, P., Morche, D. & Goldscheider, N. (2014), 'Hydrogeology of an alpine rockfall aquifer system and its role in flood attenuation and maintaining baseflow', *Hydrology and Earth System Sciences Discussions* **11**, 6805–6841.

Leibundgut, C. & Seibert, J. (2011), Tracer Hydrology, *in* 'Treatise on Water Science', Vol. 2, Elsevier Ltd, pp. 215–236.

Linsbauer, A., Paul, F. & Haeberli, W. (2012), 'Modeling glacier thickness distribution and bed topography over entire mountain ranges with GlabTop: Application of a fast and robust approach', *Journal of Geophysical Research* **117**(F3), F03007.

Magnusson, J., Kobierska, F., Huxol, S., Hayashi, M., Jonas, T. & Kirchner, J. W. (2012), 'Melt water driven stream and groundwater stage fluctuations on a glacier forefield (Dammagletscher, Switzerland)', *Hydrological Processes* **836**(3), 823–836.

McClymont, A. F., Hayashi, M., Bentley, L. R., Muir, D. & Ernst, E. (2010), 'Groundwater flow and storage within an alpine meadow-talus complex', *Hydrology and Earth System Sciences* **14**(6), 859–872.

MeteoSwiss (2015), *Climate normals for station Gütsch ob Andermatt*, last accessed on 15.03.2015.
URL: *http://www.meteoschweiz.admin.ch/home/klima/vergangenheit/klimanormwerte/klimadiagramme-und-normwerte-pro-station.html?region=Tabelle*

Moll, A. (2012), Vergangenheits- und Gegenwartsanalyse , Eisradarmessungen zum Stand 2011 sowie Modellierungen einer zukünftigen möglichen Gletscherentwicklung Zusammenfassung, PhD thesis, University of Zürich.

Moser, H., Rauert, W. & Behrens, H. M. (1980), *Isotopenmethoden in der Hydrologie*, Borntraeger, Berlin, Stuttgart.

Mueller, M. H., Weingartner, R. & Alewell, C. (2013), 'Importance of vegetation, topography and flow paths for water transit times of base flow in alpine headwater catchments', *Hydrology and Earth System Sciences* **17**(2012), 1661–1679.

Ofterdinger, U. S., Balderer, W., Loew, S. & Renard, P. (2004), 'Environmental isotopes as indicators for ground water recharge to fractured granite.', *Ground water* **42**(6-7), 868–79.

Rebetez, M. & Reinhard, M. (2007), 'Monthly air temperature trends in Switzerland 1901–2000 and 1975–2004', *Theoretical and Applied Climatology* **91**(1-4), 27–34.

Roy, J. W. & Hayashi, M. (2008), 'Groundwater exchange with two small alpine lakes in the Canadian Rockies', *Hydrological Processes* **22**, 2838–2846.

Roy, J. W. & Hayashi, M. (2009), 'Multiple , distinct groundwater flow systems of a single moraine – talus feature in an alpine watershed', *Journal of Hydrology* **373**(1-2), 139–150.

Schneider, P. (2013), 'Alpine Groundwater - Pristine Aquifers under Threat?', *Forschungskredit Uni Zürich, Research Plan* pp. 1–7.

Schneider, P. & Lange, A. (2014), 'Alpine Groundwater - Pristine Aquifers under Threat?', *AGU Poster* .

Schneider, P., Lange, A. & Doppler, T. ((in prep.)), 'Development and Evaluation of a water-level proportional water sampler', *in preparation* .

Schürch, M., Kozel, R., Schotterer, U. & Tripet, J.-P. (2003), 'Observation of isotopes in the water cycle - the Swiss National Network (NISOT)', *Environmental Geology* **45**(1), 1–11.

SLF (2014), *SLF Weekly report (21.03.-27.03.2014)*, last accessed on 15.03.2015.
URL: *http://www.slf.ch/schneeinfo/wochenbericht/2013-14/0321/index_DE*

Soilmoisture Equipment Corp. (2012), 'Operating instructions for Guelph Permeameter', pp. 1–60.

Tague, C. & Grant, G. E. (2009), 'Groundwater dynamics mediate low-flow response to global warming in snow-dominated alpine regions', *Water Resources Research* **45**(7), 1–12.

Viviroli, D., Archer, D. R., Buytaert, W., Fowler, H. J., Greenwood, G. B., Hamlet, A. F. & Huang, Y. (2011), 'Climate change and mountain water resources : overview and recommendations for research , management and policy', pp. 471–504.

Viviroli, D. & Weingartner, R. (2004), 'The hydrological significance of mountains: from regional to global scale', *Hydrology and Earth System Sciences* **8**(6), 1017–1030.

Viviroli, D., Weingartner, R. & Messerli, B. (2003), 'Assessing the Hydrological Significance of the World's Mountains', *Mountain Research and Development* **23**(1), 32–40.

Ward, J. V., Malard, F., Tockner, K. & Uehlinger, U. (1999), 'Influence of ground water on surface water conditions in a glacial flood plain of the Swiss Alps', *Hydrological Processes* **13**(April 1998), 277–293.

Wels, C., Cornett, R. J., Lazerte, B. D., Nuclear, C. R., River, C. & Branch, W. R. (1991), 'Hydrograph separation: a comparison of geochemical and isotopic tracers', *Journal of Hydrology* **122**(1), 253–274.

WRB (2006), 'World reference base for soil resources 2006', *World Soil Resources Reports* **103**.

Acknowledgment

I would like to thank the following people for their support during the thesis and the studies:

First of all my supervisor Dr. Philipp Schneider for supervision of my thesis, a lot of inspiring discussions, many ideas, suggestions as well as practical support.

Prof. Dr. Markus Weiler and Prof. Dr. Jan Seibert for being my consultants.

I am grateful for all help and support during the field & laboratory work during this thesis.
Special thanks to the two hut wardens of Albert-Heim hut, Roman Felber and Marco Traxel, for collecting the precipitation samples and the delicious meals after long field days. Thanks to Marcus and Ronnie for their support in the field. Many thanks also to Benjamin Fischer and Barbara Herbstritt for doing the isotope analysis and Lucien Biolley from ETH Zürich for conducting the ion chromatography. Furthermore, I want to thank Sandra Röthlisberger for her assistance in the laboratory and Emil Blattmann for the support during the construction of the double-packer system. For the analysis of the ERT-measurements I would like to say thanks to Christin Hilbich.

Moreover, I want to thank my parents who made it possible for me to study.

I owe my deepest gratitude to Franzi who supported me when ever she can.

Ehrenwörtliche Erklärung:

Hiermit erkläre ich, dass die Arbeit selbständig und nur unter Verwendung der angegebenen Hilfsmittel angefertigt wurde.

Freiburg im Breisgau, 31. März 2015

Unterschrift